Analytical and Isogeometric Modeling for Bending Analysis of FG and FGCNTRC Plates

A Dissertation submitted

in partial fulfillment of the requirements

for the degree of

Master of Engineering

In CAD/CAM Engineering

by

Aakash Soni

Roll.No.801584001

Under the guidance of:

Dr. Neeraj Grover

Assistant Professor

Mechanical Engineering Department

Dr. Gagandeep Bhardwaj

Assistant Professor

Mechanical Engineering Department

MECHANICAL ENGINEERING DEPARTMENT,
THAPAR UNIVERSITY, PATIALA-147004, PUNJAB, INDIA
July 2017

Certificate

This is to certify that the work done in this thesis report title **"Analytical and Isogeometric Modeling for Bending Analysis of FG and FGCNTRC Plates"** submitted in partial fulfilment of requirement for the award of Master of Engineering degree in CAD/CAM in the Mechanical Engineering department of Thapar University, Patiala, is an authentic record of work carried out by me under the guidance of **Dr. Neeraj Grover** and **Dr. Gagandeep Bhardwaj**, Mechanical Engineering department, Thapar University, Patiala. The matter embodied in this report has not been submitted in any part or full to any other university or institute for the award of any degree.

Aakash Soni

Aakash Soni

Roll No. 801584001

This is to certify that above declaration made by the student concerned is correct to the best of my knowledge & belief.

Dr. Neeraj Grover
Assistant Professor,
MED

Dated: 17/7/17.

Dr. Gagandeep Bhardwaj
Assistant Professor,
MED

Dated: 17/7/17.

Dedicated to

My nephews

Advik and Akul

You make every moment full of joy

Acknowledgement

I would like to extend a sincere and heartfelt gratitude to all those who helped me in completing, this thesis report. I would begin by thanking Dr. Neeraj Grover and Dr. Gagandeep Bhardwaj for their time, support and encouragement throughout the course of this study. I have learned so much from them and look forward to their continuous support through the future endeavours in life.

I would also like to thank my parents, family and friends for their love and moral support. Lastly, I would like to thank almighty for this opportunity and all the wonderful thing in life.

Aakash Soni

Abstract

In this study, the bending analyses for functionally graded plates is performed using the closed form and numerical solutions. Two types of functionally graded plates are considered namely the functionally graded plates with two phases and functionally graded carbon nanotube reinforced composite plates. The framework of the analysis is laid using the displacement fields from the inverse hyperbolic shear deformation theory. The principle of virtual work and Lagrange equations are used to formulate the governing equations. The linear strain-displacement relations and generalised Hooke's law are used in the formulation. The results for values of deflection and stress are validated by comparing them with the established results from the literature. The effects of factors like power law index, span to thickness ratio, aspect ratio, volume fraction and degree of curve in case of numerical analyses are considered.

Keywords: Functionally graded materials, carbon nanotubes, displacement fields, shear deformation theory, isogeometric analysis, Navier solution.

Table of Content

S. No.	Title	Page No.
	List of Figures	vii
	List of Tables	ix
	Nomenclature	xi
1.	**Introduction**	1
	1.1 Composites	1
	1.2 Functionally Graded Materials	4
	1.3 Carbon Nanotube	7
	1.4 Modelling and Analysis of Structural Elements	9
	1.5 Isogeometric Analysis	9
	1.6 Summary	11
2.	**Literature Review**	12
	2.1 Introduction	12
	2.2 Equivalent Single Layer Theory	12
	2.3 Functionally Graded Materials with Two Isotropic Phases	15
	2.4 Analysis of Carbon Nanotubes Reinforced Composites	17
	2.5 Observations From Literature	18
	2.6 Objective of the Present Work	19
	2.7 Scope of the Present Work	19
	2.8 Summary	19
3.	**Mathematical Formulation**	20
	3.1 Introduction	20
	3.2 Displacement Fields	21
	3.3 Strain-Displacement Relationship	22
	3.4 Constitutive Relations	22
	3.5 Analytical Solution for Static Analysis of Functionally Graded Composite Plate	26
	3.6 Numerical Solution for Bending Analysis of Functionally Graded Plates	31
	3.7 Summary	39

4.	**Results and Discussions**	40
	4.1 Introduction	40
	4.2 Analyses of FGM Plate with Two Isotropic Phases via Closed Form Solutions	40
	4.3 Analyses of FGM Plate with Two Isotropic Phases via Isogeometric Analysis.	45
	4.4 Analysis of FGCNT Plates Using Closed Form Solutions	48
	4.5 Analysis of FGCNTRC Plates Using Isogeometric Analysis	58
	4.6 Summary	62
5.	**Conclusion and Scope for Future Work**	63
	References	65

List of Figures

Figure No.	Figure Title	Page No.
Figure 1.1	Old and modern applications of composites (a), A chinese horse rider bow, (b) Ooypoort bridge in Nijmegen, the Netherlands, (c) Material distribution in an airbus A380.	3
Figure 1.2	Types and applications of FGMs	5
Figure 1.3	Pore gradation in human bone.	6
Figure 1.4	Atomic structure of a graphene sheet	8
Figure 1.5	Types of CNTs (a) cut-out part of graphene sheet (b) SWCNT (c) MWCNT.	8
Figure 2.1	Difference between CPT, FSDT and TSDT according to the shape, size and orientation of the transverse normal.	13
Figure 3.1	Coordinate system and dimensions of the two phase FGM plate.	20
Figure 3.2	Distribution scheme and dimensions of the FGCNRTC plate.	21
Figure 3.3	Basis functions for a quadric curve for a knot vector $\Xi = [0\ 0\ 0\ 0.25\ 0.50\ 0.75\ 1\ 1\ 1]$.	34
Figure 3.4	Control points and elements for NURBS (a) *p*=1 (b) *p*=2.	35
Figure 4.1	Variation of normal stress with non-dimensional thickness for a functionally graded plate with *a/h*=10 under sinusoidal loading	43
Figure 4.2	Variation of non-dimensional displacement with span ratio for SSL and UDL loading and *N*=1.	43
Figure 4.3	Variation of non-dimensional transverse displacement with the power law index under sinusoidal loading.	44
Figure 4.4	Variation of non-dimensional transverse shear stress along the thickness direction for simply supported FGM plate.	45
Figure 4.5	Effect of degree of basis function on rate of convergence for a functionally graded plate with *N*=1	46
Figure 4.6	Effect of span to thickness ratio on the rate of convergence for IGA analyses with basis functions of degree *p*=2	46

Figure 4.7 Effect of power law index N on the convergence rate for the IGA analyses of a FGM plate with *a/h*=10 47

Figure 4.8 Variation of non-dimensional axial stress $\sigma_{xx}(a/2, b/2, z)$ with non-dimensional depth (*z/h*) 56

Figure 4.9 Variation of non-dimensional transverse shear stress $\bar{\tau}_{yz}(a/2, 0, h)$ with non-dimensional thickness for thickness ratio *a/h*=50 and a CNT volume fraction of $V_c^* = 0.11$ under sinusoidal loading. 57

Figure 4.10 Variation of non-dimensional axial deflection with span to thickness ratio for a FGCNTC platefor uniformly distributed and sinusoidally varying loads, (a) UD (b) FGVCNT (c) FGOCNT (d) FGXCNT. 58

Figure 4.11 Effect of CNT distribution scheme on the convergence rate for a FGCNTRC plates with *b/h*=10 and $V_c^* = 0.11$. 59

Figure 4.12 Effect of CNT distribution scheme on the convergence rate for a FGVCNTRC plates with *b/h*=10. 59

List of Tables

Table No.	Table Title	Page No.
Table 3.1	Fourier series expansion coefficients for different loading conditions in Navier method	30
Table 4.1	Validation of non-dimensional stresses and displacement for a square plate with a/h=10	41
Table 4.2	Validation of non-dimensional transverse deflection for FGM plate with a/h=10 for FGM plate with exponential variation of properties	42
Table 4.3	Non-dimensional deflection for IGA of FGCNTR composite square plates with p=1	48
Table 4.4	Efficiency parameters of SWCNT	49
Table 4.5	Variation of non-dimensional central deflection w/h with CNT volume fraction V_c^* and width to thickness ratio (b/h) under a uniformly distributed load of $q_0=1\times10^5$ N/m^2	50
Table 4.6	Effect of CNT addition for a square plate with b/h=100 under hydrostatic loading load of $q_0=1\times10^5$ N/m^2	51
Table 4.7	Non dimensional central deflection and stresses for a simply supported rectangular plate under uniformly distributed load of $q_0=1\times10^5$ N/m^2	52
Table 4.8	Non dimensional central deflection and stresses for a simply supported rectangular plate under Hydrostatic loading with a maximum load of $q_0=1\times10^5$ N	53

Table 4.9	Non dimensional central deflection and stresses for a simply supported rectangular plate under a sinusoidal load of q_0=1×10^5 N	54
Table 4.10	Non dimensional central deflection and stresses for a simply supported rectangular plate under central point load with q_0=1×10^5 N	55
Table 4.11	Non dimensional central deflection for a square FGCNTRC plate with V_c^*=0.11 under different boundary conditions	60
Table 4.12	Non dimensional deflection for a FGCNT reinforced plate with volume fraction 0.14 and under a uniformly distributed load of q_0=1×10^5 N	61
Table 4.13	Non dimensional deflection for a FGCNT reinforced plate with volume fraction V_c^*=0.17 under a uniformly distributed load of q_0=1×10^5 N	61

Nomenclature

x, y	Cartesian coordinate directions
u, v	In-plane displacements
$w, \overline{w}$	Dimensional and non-dimension deflection
u_0, v_0, w_0	Mid-plane displacements
a, b, h	Length breadth and thickness of the plate
N	Power law index
V_c	Volume fraction of CNT
Q	Transformation matrix
E	Elasticity Constant
G	Rigidity matrix
U	Strain energy
W	Work done
$\{F\}$	Force vector
R	Resultant stiffness matrix
Q	Transverse load
p	Degree of B-spline basis function

Greek Symbols

θ_x, θ_y	Shear rotations
$\varepsilon_x, \varepsilon_y$	In-plane normal strains
γ_{xy}	In-plane shear strains
γ_{yz}, γ_{xz}	Transverse shear strain
τ	Shear stress
Δ	Generalised displacement vector
$\hat{\xi}, \hat{\eta}$	Coordinate axis in parent element
ξ, η	Coordinate axis in parametric space
ν	Poisson’s ratio

Acronyms

CLPT	Classical laminated plate theory
CNT	Carbon nanotubes
FGM	Functionally graded materials
FGCNTRC	Functionally graded carbon nanotube reinforced composites
FEA	Finite element analysis
FSDT	First order shear deformation theory
HSDT	Higher order shear deformation theory
IGA	Isogeometric analysis
IHSDT	Inverse hyperbolic shear deformation theory
SSL	Sinusoidal load
UDL	Uniformly distributed load

Chapter 1

Introduction

The success of the human civilisation is based on its continuous thrust towards being better in every aspect of life. It is our desire to be connected, to be faster, to fly that lead to modern marvels like internet mobile phones supercars aeroplanes etc. most of these wonders are made of and are fuelled by conventional energy sources. But as science progresses the world has come to realisation that judicious and better use of these materials is required for examples vehicles are required to consume less fuel and still be fast, modern sports utensils are needed to be lighter but have increased strength etc. the above mentioned changes along with human curiosity have led to the introduction and growth in the field of advanced engineering materials. Composites and alloys are two of the examples of such materials. Idea of a composite material arises from need of materials which can superior material properties and can still be extremely light in weight. Such requirements are very common in aerospace, automotive and aviation industries. Aerospace industry also developed the functionally graded materials as these materials have excellent thermal resistance and are used in spacecraft as thermal shields. Another requirement arose from the biomedical field of where naturally occurring materials can’t be used in implants as they didn’t have the required microstructure to mimic the properties of a living tissue. All this and many other factors have led to the development of the concept of composites.

1.1. Composites

The composites can be defined as materials obtained by combining of two or more materials at a macroscopic level. The primary objective is to produce a material which has superior engineering properties as compared to any of the two parent elements. For example they have superior stiffness, strength, toughness, fatigue life etc. at a considerably lower weights. Because of these superior properties human beings have been using composites for a long time. The earliest examples includes bricks made with straws as reinforcements in a matrix of mud. Another example is the bows used by ancient Asian warriors to shoot down enemies while riding a horse, which were nothing but a laminated composite. An example of such a bow is given in Figure 1.1(a) Today composites find their applications in all walks of life ranging from porcelain cement to RCC (Reinforced concrete cement) roofs and the material used to manufacture body of aeroplanes (see Figure 1.1(b)), sports cars, ships, space ships, and even cycles and sports equipment. Today bridges completely made out of fibreglass are being used in many European cities as motorways and as footbridges (see Figure 1.1(c)).

Typically a composite consists of two phases: binder or matrix and reinforcements or fillers. The matrix holds the reinforcements in place, facilitates load transfer between fibers and shields the fibers from corrosive environment. Fibers usually have better strength and stiffness as compared to bulk form of the same material, for example the Young's modulus for E Glass fiber is 73 GPa. Due to their superior mechanical properties fibers take most of the load applied to the structure and are the primary reason for higher strength and stiffness. Since the properties of the composite depends upon the properties of matrix and reinforcement, composites can be tailor made by selecting different combinations of matrix and reinforcements. Nano particles like carbon nanotubes (CNT) when used as reinforcement yields composites with superior properties, such composites come under the category of Nanocomposites. A composite is usually classified in three categories: (1) Fibrous Composites, where fibers are used as reinforcements in a matrix, (2) Particulate Composites, which comprises of macromolecules of a material in a matrix of some other material and (3) Laminated Composites are made by stacking together layers (called laminas) one over the another in particular sequence. These layers can be of metal, non-metal or of a composite of any of the above mentioned kinds. The composites can further be classified as wooven, unidirectional, bidirectional or randomly arranged depending upon its fiber orientation. Unidirectional composites will display better properties like strength and modulus in the fiber direction but are susceptible to failures due to fiber pull out, breakage in fiber and fiber bucking due to poor properties in the transverse direction.

1.1.1 Laminated composites

A laminated composite is a collection of different laminae stacked one over the other in such a manner that the desired properties are achieved in a specific direction. A lamina can be a layer of metal, non-metal or even a layer of composite material. In cases where the laminae are fibrous composites, the order of the fiber orientation in laminae is termed as stacking sequence or lamination scheme. This stacking sequence can be decided according to the stress conditions in the application of the composite. For example if a laminate is required to bear predominately shear load than layers with fibers oriented with angles of 30^0 or 45^0 will be best suited.

Despite the above mentioned advantages laminated composites suffer from certain shortcomings such as delamination, fiber debonding and manufacturing defects like interlaminar voids, damaged fibers, variation in thickness, etc. Delamination is a mode of failure in composite materials where the layer of laminate separate at a particular point resulting in formation of mica like surface and a significant decrease in the toughness of the composite. These problems has led to the development of other materials to obtain the required gradation of properties and has given birth to new kind of advanced engineering material known as functionally graded materials.

(a) (c)

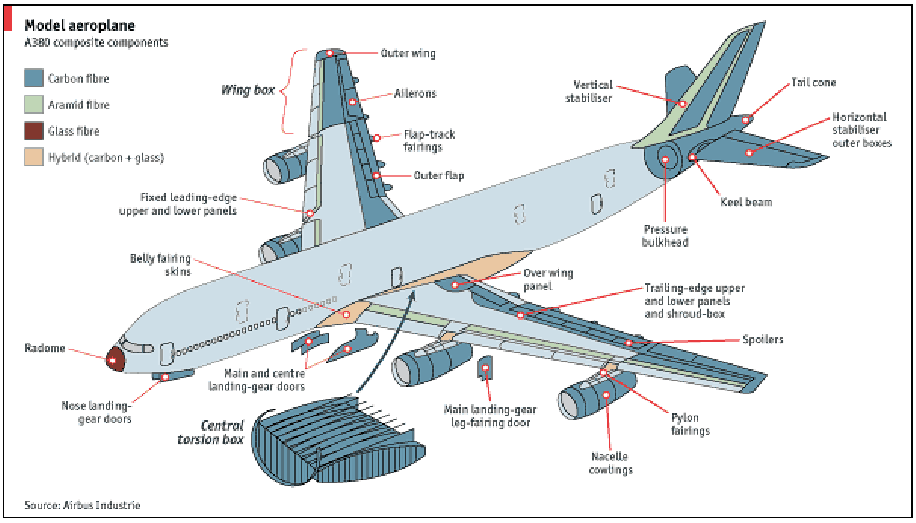

(b)

Figure 1.1 Old and modern applications of composites (a)An asian horse rider bow, (b) Material distribution in an airbus A380, (c) The Ooypoort bridge in Nijmegen, the Netherlands

(a) https://upload.wikimedia.org/wikipedia/commons/c/c5/KaiyuanBowStrung.jpg

(b) http://d2n4wb9orp1vta.cloudfront.net/cms/IMG_4992_500.jpg;width=560

(c) http://www.compositesworld.com/news/dutch-bridge-claims-to-be-largest-single-span-composite-bridge-in-the-world

1.2. Functionally Graded Materials (FGMs)

In functionally graded (FG) materials, the material properties are continuously varied as a function of space in a specified dimension by mixing two different materials and thus no internal boundaries exist in such materials. The absence of internal boundary between phases ensures that there is no issue of stress concentration at the phases of different boundaries. The gradual change of material properties may be tailored to suit different working conditions.

1.2.1. Types of functionally graded materials

Functionally graded materials can be categorized depending upon the manner in which the gradation of properties is achieved.

(a) **Gradation in chemical composition of the material:** These are most common type of functionally graded materials. One of the most common ways of achieving a continuous gradation of properties include mixing of two isotropic material phases by the help of powder metallurgy. The most common example of such kind is where one of the phases is an engineering alloy of magnesium, aluminum, copper, titanium etc. and the other phase is one of the advanced ceramic materials like zirconia, alumina and tungsten carbide etc. Another method to achieve the required gradation includes varying the composition or the distribution of reinforcements in the composite. This method has gained popularity in recent times as it allows better control over property variation. One of the examples of this kind, functionally graded carbon nanotube reinforced composite plate is discussed in details in later sections.

(b) **Gradation in porosity:** Mother Nature has provided us with variety of naturally occurring composite materials, FGMs with gradation in porosity is one of them. Gradation in properties due to porosity can be achieved either by varying the pore density in one of the directions in space or by increasing or decreasing the size of the pores in one of the directions. This not only directly effects the material properties like toughness, strength etc., but also impacts the mass and application of the component.

(c) **Gradation in microstructure:** In this class of FGMs, the microstructure of the material is tailored to obtain specific properties in the composite. One of the ways to achieve this kind of gradation is to different cooling techniques at different location to achieve the required variation in microstructure. For example the outermost layer might be quenched making it very hard at the surface while the core can be allowed to cool down slowly hence causing a variation in the microstructure of the material.

1.2.2. Examples and Applications of functionally graded materials

(a) Naturally occurring FGMs: The concepts of functional gradation of material properties might be new to human kind, but nature is filled with examples of such materials. Bones for example has a smooth gradation of porosity where the pore size and pore density varies with the thickness of bones, to facilitate the path for blood vessels. The joints between ligament and bones is another example of functional gradation of material where there is a functional gradation of collagen and other minerals from soft ligament tissue to hard bone tissues.

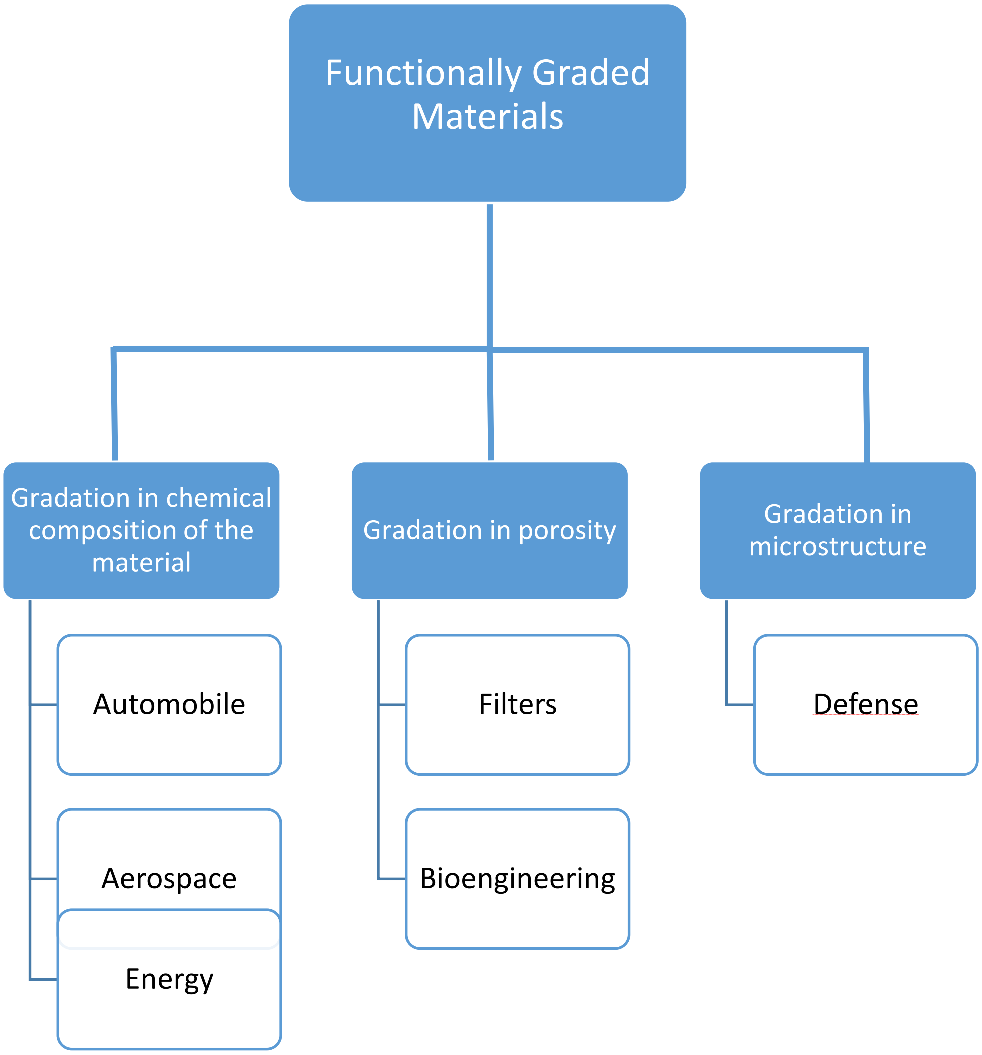

Figure 1.2 Types and applications of FGMs

Human skin is another example of functionally graded material where the gradation helps to achieve the required combination flexibility and toughness, at the same time having enough pore density for sweating. Other examples include leafs and branches of trees, ligaments, igneous rocks, earth's crust among, etc.

(b) Artificial FGMs: The functionally graded materials with variation in composition act as great thermal barriers, with the ceramic side facing the corrosive or high temperature environment and the metal part where the requirement is of high mechanical properties. This is due to the fact that no stress concentration occurs as there are no boundaries between different phases and stress distribution is smooth. Functionally graded materials of this kind find their application in places where high temperature and highly corrosive environments exist such as thermal shields in aircrafts and space shuttles, in thermal and nuclear power plants. The coating of FG material is provided at the tip of the spacecraft so as to reduce the thermal stresses when it renters into the earth's atmosphere, hence it can take the high thermal and shear stresses that arise due to extreme friction and aerodynamic heating. Types and applications of functionally graded materials can be understood with the help of Figure 1.2.

Functionally graded materials with gradient due to porosity find their applications in the medical fields, such as the implants which are made to mimic the actual body tissues and most of the tissues in our body are functionally graded with respect to porosity. The pore gradation in a human bone is shown in Figure 1.3

Other applications include automotive industry, defense industry, communication sector where the optical fibres are treated as functionally graded materials and sports to name a few.

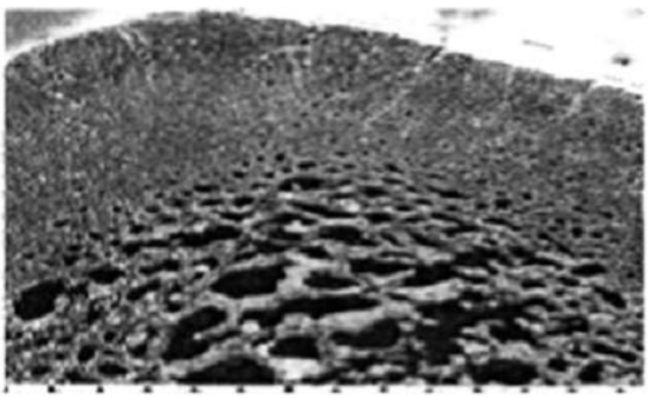

Figure 1.3 Pore gradation in human bone. (Jha *et al*. 2013)

1.3 Carbon Nanotubes

Since its invention in 1991 by Sumio Iijima (Iijima 1991), the carbon nanotubes have gained considerable popularity in various engineering fields due to their exception mechanical and thermal properties. The carbon nanotubes can be thought of as cylindrical macromolecule consisting of carbon atoms arranged in a periodic hexagonal structure.

Carbon Nanotubes have excellent mechanical, thermal and electrical properties. The elastic modulus for these tubes is theoretically and experimentally found to be greater than 1 TPa (elastic modulus for diamond is 1.2 TPa). The strengths 10-100 times higher than strongest of the steels. Additionally, the CNTs are thermally stable at temperatures up to 2800℃, have thermal conductivity twice that of diamond and a current carrying capacity 1000 times higher than copper wire (Thoteson 2001). The CNTs due to their smaller size can be assumed to fall in the category of whiskers and thus have better properties than the traditionally used carbon fibres.

When these nanotubes are used in composite material as reinforcements they lead to the formation of nanocomposites with significantly better engineering properties. Studies have concluded that the Young's modulus and the yield strength of composite is doubled by adding 1% CNT by weight and quadrupled with 4% CNT by weight (Thoteson 2003). The CNT-reinforced composite materials may be used in the form of beam, plate, or shell as structural components. Thus, investigating mechanical responses of structures made of CNT-reinforced materials is important.

1.3.1 Structure of carbon nanotubes

CNTs be visualised as single or multiple sheets of graphene rolled to form a tube-like structure. Graphene is formed as a 2-D sheet of carbon atoms arranged in a hexagonal array. In this case, each carbon atom has three neighbours. The properties of the CNT's are affected by the atomic arrangement, length and diameter of the carbon nanotubes. The atomic structure of graphene is shown in Figure 4.

The structure of CNTs is defined on the basis of chirality of the tube. Chirality, in turn, is described by a chiral vector and chirality angle. The chiral vector C_h can be determined by:

$$C_h = n\overrightarrow{a_1} + m\overrightarrow{a_2} \quad (1.1)$$

where, *n* and *m* are the number of steps along the zig zag carbon bonds of the hexagonal carbon lattice and $\overrightarrow{a_1}$, $\overrightarrow{a_2}$ are the unit vectors. Chiral angle determines the amount of twist in the tube.

There exist two limiting cases with chiral angle equal to 0° and 30°. These two cases are referred to as zig zag (0°) and arm chair (30°). In terms of roll up vector arm chair would be (n, n) while zig zag would be (n, 0).

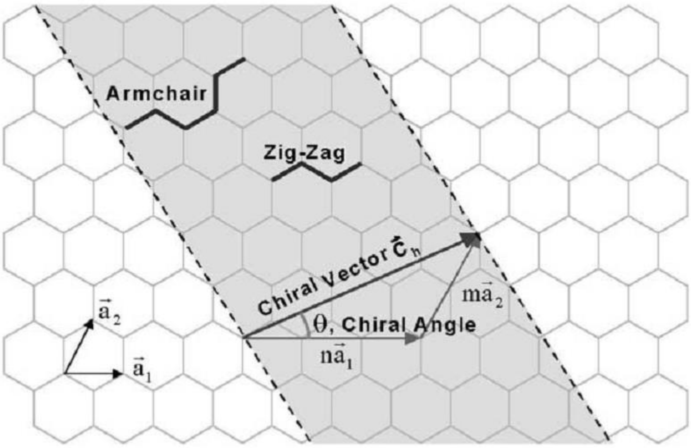

Figure 1.4 Atomic structure of a graphene sheet (Thoteson 2001)

1.3.2 Types of Carbon Nanotubes

The CNTs can be differentiated on the basis of number of rolled up graphene sheets used to make the nanotube:

Single-walled CNT: If a single rolled up graphene sheets is used to manufacture the nanotube then it is called Single-walled CNT (SWCNT).

Multi-walled CNT: If multiple rolled up graphene sheets are used to manufacture the nanotube then it is called Multi-walled CNT (MWCNT). These classifications are indicated in Figure 1.5.

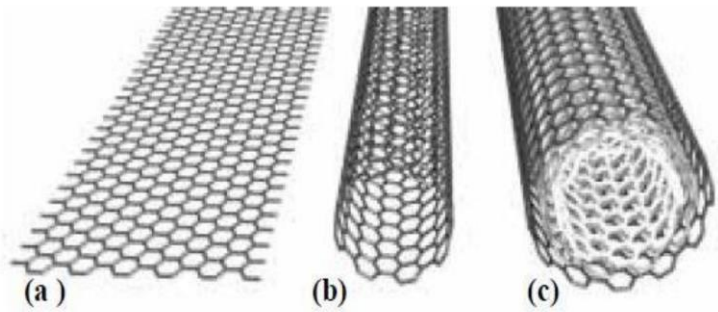

Figure 1.5 Types of CNTs (a) cut-out part of graphene sheet (b) SWCNT (c) MWCNT (Kreupl *et al.* 2003)

1.4. Modelling and Analyses of Structural Members

Structural members like beams, plates and shells are studied to evaluate their behaviour in different environments based on the application. Two basic steps while performing such analyses is deriving the governing equations and solving these governing equations. For structural analyses the governing equations are found with the help of carefully chosen displacement fields and some basic laws of physics and mechanics. Methods commonly used for solving governing equations of such members can be classified into two fractions (1) Methods to obtain exact solutions (2) Methods to obtain numeric solutions. While the exact methods would yield more accurate results, they are not very easy to calculate and in some cases it might not be even possible to find these solutions. To solve this problem numerical methods have been developed over the years. One of the most common method is the Finite elements method, which can solve most complex of the problems to a certain degree of accuracy by dividing the domain into smaller elements and developing equations for these smaller elements. These elemental solutions are then clubbed to arrive at a final solution for the whole system.

1.5. Isogeometric Analysis

Isogeometric analysis (IGA) is a computational technique that utilises the concepts of computer aided design and computer aided engineering (CAE). It utilises the geometric elements described with the Non-uniform rational B-spline (NURBS) basis functions directly for the purpose of analyses. The use of NURBS basis function in analyses allows the user to obtain better results even with a coarse mesh.

1.5.1 Computer aided engineering (CAE)

Computer aided engineering is a tool to reach optimum design solutions and perform analyses and simulations with the help of a computer software. Finite element analyses has been a major forerunner in industries as the background computational method for most of these software packages. Finite element analysis was developed in 1950s and 1960s to suit the analysis requirements of the aerospace industry and soon found its application in almost all the fields of engineering and science. Late 1960s saw the development of the first FEA computer program for commercial purposes. Basic steps involved in finite element analyses include discretisation or mesh generation followed by obtaining element level equations and assembling and solving those equations with the help of boundary conditions to obtain the required results. In the discretisation step the domain of the problem is divided into simple non-overlapping elements. Line elements for 1-D problems, Triangular and quadrilateral elements for 2-D problems and tetrahedral and hexahedral elements for 3-D problems are some of the examples of such elements. The basis functions used in the analyses are usually Lagrangian and hermite polynomials. Different variational methods along with differential equations to for the given kind of problem are used to formulate the problem as linear equations. These equations are then solved with the help of boundary conditions and matrix algebra.

1.5.2 Computer aided design (CAD)

Computer aided design is the engineering field where the models and drawing of the required part is made with the help of computers. Before the invention and evolution of computers the drawings were created by hand on a sheet with help of different geometric instruments. This changed from year 1966 onwards when the use of computers for the purpose of design and drawing became possible. Use of computers made possible not only creating drawings with better accuracy and readability in a greatly reduced time but also made possible creating realistic 3-D models. 1975 saw the beginning of use of Non-uniform Rational B-splines (NURBS) in CAD programs. Advantages of using NURBS lies in its simplicity and flexibility to represent different curves and surfaces. They provide the option of local control of the geometry where a portion can be manipulated using kont vectors. The continuity can be easily controlled by varying the order of the curve. The NURBS basis functions can be used to generate free form surfaces with relative ease and can exactly represent all the conic sections.

In most of the design and analysis packages these days the geometric data set obtained from CAD package is first converted into a data set suitable for FEA analysis and this conversion can be termed as mesh generation. In such systems 80% of total analysis time is consumed in mesh generation and yet the mesh obtained is only an approximation of the given geometry. This leads to geometric errors in the solutions. In modern day engineering components with increasingly complex geometries are required and their analysis without a due consideration to the geometry is getting lesser and lesser acceptable.

As a link between engineering design and analysis Hughes *et al.* (2005) introduced the concept of isogeometric analysis**,** where the emphasis is to develop a method of analyses using a precise geometric representation. The basis of isogeometric analysis is to develop a CAD model whose data set can be directly used for analysis without first having to convert the data set in a FEA suitable data set. The focus while developing an IGA formulation is on exact representation of the geometry of the object. Since its introduction isogeometric analysis has garnered huge amount of interest in the engineering community especially in European countries with multi-million dollar projects like EXCINTING and ICADA being floated to develop isogeometric analysis as a prominent method of analysis in design industry.

1.6. Summary

The development and requirement of advanced materials for various applications is stated in this chapter. Functionally graded materials and functionally graded carbon nanotube reinforced structures find potential applications in the structural design. Moreover, the modelling and analyses of such structures in the framework of advanced CAD software is the type of development which can be foreseen.

Chapter 2

Literature review

2.1 Introduction

This section explains some of the works done in the field of functionally graded materials in the available literature. Studies for functionally graded materials with two isotropic phases and functionally graded carbon nanotube reinforced composite structures have been presented in this section. This section also deals with different equivalent single layer (ESL) theories and formulation frameworks. Research on both analytical and numeric solving techniques are discussed to provide an insight into the work that has been accomplished in the given field.

2.2 Equivalent Single Layer Theories

Exact three dimensional (3-D) solutions for the structural analysis of materials have been provided by Pagano (1970), Srinivas and Rao (1970) and Srinivas *et al*. (1970). Despite their accuracy for finding the exact solutions these approaches involve higher computational cost and it is very difficult to find these solutions for certain cases. This led to the development of equivalent single layer theories (ESL). ESL theories treat a 3-D continuum problem as an equivalent 2-D problem to simplify the formulation.

The simplest and first one among the ESL theories is the classical plate theory (CPT) given by Love (1927) which is based upon the Kirchhoff's hypothesis about the transverse normal and shearing strains. Reissner and Stavwsky (1961) implemented the classical plate theory for laminated structures and gave it the name of classical laminated plate theory (CLPT). According to CLPT the displacement fields are written as

$$u(x,y,z) = u_0(x,y) - z\frac{\partial w_0}{\partial x}$$

$$v(x,y,z) = v_0(x,y) - z\frac{\partial w_0}{\partial y}$$

$$w(x,y,z) = w_0(x,y) \qquad \text{(2.1a-2.1c)}$$

where, u_0, v_0, w_0 are the midplane displacements in the coordinate directions.

The CLPT completely ignores the presence of transverse strains which gives certain inaccuracies, but still CLPT produces good results for the case of thin plates. Some of the shortcomings of the CLPT were overcame by Reissner (1945) and Mindlin (1951), when they studied the impact of transverse shear strain and proposed the first order shear deformation theory (FSDT). According to FSDT the displacement fields are given as

$$u(x, y, z) = u_0(x, y) + z\emptyset_x$$

$$v(x, y, z) = v_0(x, y) + z\emptyset_y$$

$$w(x, y, z) = w_0(x, y) \qquad (2.2a\text{-}2.2c)$$

where, $\emptyset_x, \emptyset_y$ are the rotations about y and x axis respectively. Though FSDT considers the effect of transverse shear stress but it assumes its value to be a constant and a shear correction factor has to be calculated to make the value of transverse shear stress equal to zero at the top and bottom surfaces of the plate. But calculating the value of shear correction factor can be a challenging task in some cases and the distribution of transverse stress comes out to be linear.

Both the CLPT and FSDT give satisfactory results for thin plates but they were found lagging when it comes to thick plates, this led to development of higher order shear deformation theories (HSDT). The HSDTs can be further classified into polynomial and non-polynomial shear deformation theories. The difference between the CLPT, FSDT and HSDTs is explained in Figure 2.1 with respect to the condition on transverse strain.

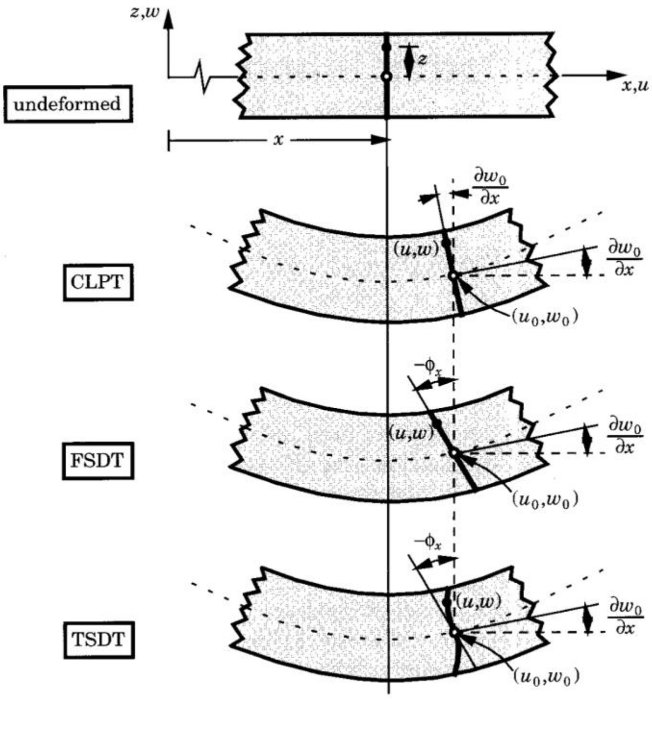

Figure 2.1 Difference between CPT, FSDT and TSDT according to the shape, size and orientation of the transverse normal. (Reddy 2004).

2.2.1 Polynomial shear deformation theories

Polynomial shear deformation theories incorporate the transverse shear strain effects by the help of polynomial coefficients of higher order terms in the Taylor series expansion of the displacement fields.

Reddy (1984) proposed a higher order shear deformation theory (HSDT). A polynomial function was chosen as the coefficient of higher order terms in the displacement field equations. This coefficient ensured that there was no residual stress at the top and the bottom layers of the composite and hence no requirement of the shear correction factor arises.

Kant *et al.* (1988) proposed a higher order shear deformation theory involving 11 variables in the Taylor series expansion of the displacement fields. They used the proposed theory to study the dynamic behaviour of isotropic and composite plates.

Murthy (1981) developed a polynomial higher deformation theory and applied it to study bending behaviour of laminated and isotropic plates.

Swaminathan and Patil (2007) performed static analysis over a cross-ply laminated plate and a sandwich plate using a higher order shear deformation theory involving 11 variables.

2.2.2 Non-polynomial shear deformation theories

Non polynomial shear deformation theories assume the variation of transverse shear strain with the help of non-polynomial function. The condition for zero transverse shear stress at the top and the bottom surfaces is satisfied without the help of a shear correction factor and realistic variations of shear strain across the thickness can be observed.

Touratier (1991) developed a theory with sinusoidal coefficient of shear strain for the analyses of composite plates.

Aydogdu (2008) formulated a non-polynomial shear deformation theory having an exponential function of thickness co-ordinate. Results for bending, free vibration and buckling analysis under transverse load, for cross ply simply supported composite plates is presented.

Mantari *et al.* (2012) developed a trigonometric shear deformation theory with a tangential shear strain coefficient. He obtained results for static and vibrational analyses of laminated and sandwich plates.

Grover *et al.* (2013) developed an inverse hyperbolic shear deformation theory for the analysis of laminated and sandwich structures. The theory uses an inverse hyperbolic sine function to express the variation of shear strains.

Grover *et al.* (2013) presented an inverse trigonometric shear deformation theory with a cot inverse function in thickness direction for the analysis of laminated and sandwich structures. The theory was applied to generate results for static and buckling analysis of composite plates.

2.3 Functionally Graded Materials with Two Isotropic Phases

Due to the easy tailorability of their properties FGMs have been a subject of extensive research. Japanese scientist introduced the world to the notion of FGMs in 1984. Extensive reviews of literature of FGMs have been carried out by Jha *et al.* (2013) and Birdman and Byrd (2007). These reviews contains details on manufacturing, application, heat transfer issues and modelling of FGM for static, dynamic and fracture analysis of FGM plates.

2.3.1 Analysis of FGM structures with two isotropic phases using 3-D elasticity solutions

Kashtalyan (2004) has given exact 3-D solutions for bending problem in an exponentially graded FGM plate subjected to simply supported boundary condition. The governing equations are solved using the Pelvako solutions for inhomogeneous isotropic media. The variation of displacement and stresses with parameters like thickness to length ratio for different values of exponential constant is considered.

The work of Kashtalyan is further extended by Zenkour (2007). He obtained solutions using the 3-D Pelvako solutions and presented a comparison with 2-D solutions obtained using a trigonometric plate theory. Values of stresses and displacements for different values of span to thickness ratio, aspect ratio and exponentially graded parameter are listed. A comparison is drawn between 2-D and 3-D results.

Pan (2003) implemented Pagano's 3-D solutions to multi-layered FGM plates, to obtain results for bending behaviour of such plates. The properties are assumed to vary according to the exponential law.

2.3.2 Analysis of FGM structures with two isotropic phases using ESL theories (Closed form solution)

Feldman and Aboudi (1997) presented buckling analysis of the FGM plates using the classical plate theory. Material gradient is taken according to a spatial distribution of the local reinforcement volume fraction. Problem was analysed using a combination of micromechanical and structural approach. The study included results on the effect of length to width ratio and different types of boundary conditions.

Javaheri (2002) studied the buckling response of functionally graded plates under in-plane loading, with the help of CPT. The properties of the plate were assumed to be exponentially graded in the thickness direction.

Praveen and Reddy (1998) studied the behaviour of a functionally graded plate under thermomechanical loading. Graphs of deflection and stress with different parameters are plotted to study the impact of different parameters on the FGM plate. A FSDT and von Karman theory are used to define the displacements and strains. Material properties are graded according to the power law.

Zenkour (2006) presented a static analysis of FGM plates with help of a trigonometric higher order shear deformation theory. Power law was implemented to calculate the properties of the plate at a given thickness and the governing equations were solved using Naviers conditions. Impact of factors like span to thickness ratio, aspect ratio and power law factor is studied on stress and displacement values.

Mantari *et al.* (2011) presented solutions for bending response of a functionally graded plate with the help of Navier conditions for a simply supported plate. The displacement fields are summed as a combination of sinusoidal and exponential functions and the properties of the plate were assumed to vary according to the power law.

Thai and Kim (2013) used a polynomial HSDT for bending and free vibration analyses of FGM plates. Power law, Hamilton's principle and generalised Hook's law were used to arrive at the governing equations which were then solved with the help of Navier's solutions for simply supported plates.

Inverse trigonometric shear deformation theory was used to study the bending and buckling behaviour of FGM plates by Kulkarni et al. (2015). Results for variation of properties according to exponential law and power law are presented and values are compared with those available in literature.

2.3.3 Analysis of FGM structures with two isotropic phases using ESL theories (Numerical methods)

Chi and Chung (2006) studied the behaviour of FGM plates under transverse loading using classical plate and theory. They obtained and compared the analytical and numeric results. Material distribution was assumed according to power law, sigmoid law and exponential law.

Talha and Singh (2010) proposed a Polynomial higher order shear deformation theory to study bending and vibration behaviour of functionally graded plates. A nine noded element is used for the analyses and results are presented for different boundary conditions.

Croce and Venini (2004) examined the static response of a FGP using the FSDT model and the variational approach. A finite element model is generated to solve the problem. The gradation of properties is according to the power law.

Valizadeh *et al.* (2013) developed an isogeometric formulation for the analysis of functionally graded plates. The FSDT is used to define the displacement fields and results are presented for different boundary conditions.

Tran *et al.* (2013) presented an analysis of functionally graded plates using NURBS basis functions using a higher order shear deformation theory. They presented results for static and vibrational analysis of FGM plates. Mori Tanaka approach was used to determine the properties of the plate.

2.4 Analysis of Carbon Nanotube Reinforced Composites

A comprehensive review of current developments in the field of functionally graded carbon nanotube reinforced composites is written by Leiw *et al*. (2015). All the current developments in the field of structures having carbon nanotube as reinforcements in functionally graded manner is presented.

Shen (2009) presented nonlinear bending analysis of isotropic matrix reinforced with functionally graded carbon nanotube reinforced composite (FG-CNTRC) plates in the thickness direction in thermal environments. Molecular dynamics is used to find the appropriate laws to define the properties.

Formica *et al.* (2010) formulated a continuum model using Eshelby-Mori-Tanaka approach to study the vibrational response of carbon nanotube reinforced (CNTRC) plates.

Static and free vibration of FG-CNTRC plates was presented by Zhu *et al.* (2012) based on first order shear deformation theory and Finite element method.

Alibeigloo and Leiw (2013) discussed the thermoelastic behaviour of functionally graded carbon nanotube reinforced composite plates under thermal environment using three dimensional theory of elasticity under thermomechanical loads.

Functionally graded CNTs are also used as a reinforcement in the case of shells and beams. Static and dynamic analysis of carbon nanotube reinforced functionally graded cylindrical panels was examined by Zhang *et al.* (2014) using first order shear deformation shell theory and Eshelby-Mori-Tanaka approach to determine the equivalent material properties of the shell. Arani *et al.* (2015) studied the distribution of stresses in CNTRC cylinder under thermo-mechanical loading in the presence of electric and magnetic fields.

Aragh *et al.* (2012) studied the vibrational characteristics of oriented and aligned carbon nanotubes using Eshelby-Mori-Tanaka scheme and generalised quadrature method.

Bhardwaj *et al.* (2013) studied the impact of CNT fraction and aspect ratio on flexural and dynamic response on laminated composite plates using Halpin-Tsai model and Chebyshev polynomials.

Natarajan *et al.* (2014) presented a bending and free vibration analyses of sandwich plates with facesheets reinforced with CNTs using a higher order structural theory and a homogeneous core.

Mehrabadi *et al.* (2012) studied the mechanical buckling of FG-CNTRC under uniaxial and biaxial loading using FSDT. The material properties were evaluated with the help of MD simulations.

2.5. Observations from Literature

- It is observed from the literature that IHSDT has not been implemented for the analysis of functionally graded plates
- Limited work on FGM analyses with isogeometric framework is available in literature.
- It is observed that there is abundant work on the evaluation of properties of CNT. However, the studies relevant to prediction of response of CNT reinforced structures are very limited. They have been modelled using FSDT or polynomial based SDT in the existing literature

- The isogeometric approach is implemented for the modelling and analysis of isotropic and composite plates in the past. The evaluation of response characteristics of FGCNTRC plates in isogeometric framework may be additional contribution in the development of isogeometric analysis.

2.6 Objective of Present Work

The objective of present work is to study the bending response of two phased functionally graded plate and functionally graded carbon nanotube reinforced composite plate under analytical and isogeometric framework.

2.7 Scope of the Present Work

- Analytical modelling of a FGM plate with two isotropic phases for bending analysis.
- Isogeometric modelling of a FGM plate with two isotropic phases for bending analysis.
- Analytical modelling of a FGCNTRC plates for bending analysis.
- Isogeometric modelling of a FGCNTRC plates for bending analysis.

2.8 Summary

A detailed literature survey is carried out focussing on the modelling and solution procedures for FG and FGCNTRC plates. The literature gaps in the existing literature are identified on the basis of observations from the literature survey and on that basis, the objectives and scope of the present work are framed. The study of existing literature also helped to understand and implement the methodologies in the desired manner.

Chapter 3

Mathematical Formulation

3.1 Introduction

This section gives an insight into the modelling of a functionally graded and functionally graded carbon nanotube reinforced composite plate using inverse hyperbolic shear deformation theory. Formulation is done with the help of principle of virtual work for the case of analytical solutions and with the help of Lagrangian equations in the case of isogeometric analysis. The solutions of those governing equations are found using Navier's closed form solution and isogeomatric analyses.

Figure 3.1 shows the plate under consideration for the analysis of the FGM. The coordinate axis is assumed at the mid plane and analyses is done in Cartesian coordinate system. The dimensions of the plate are $a \times b \times h$ in x,y,z directions respectively. Static analysis is performed for a transverse loads $q_0$for different boundary conditions under sinusoidal and uniformly distributed loading conditions.

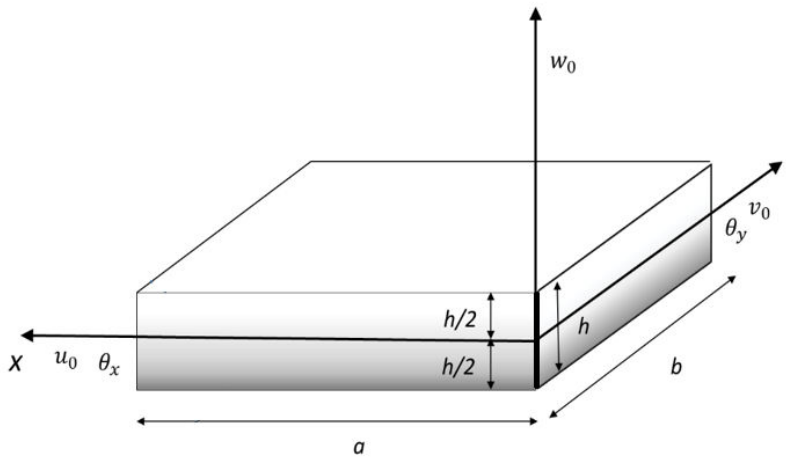

Figure 3.1 Coordinate system and dimensions of the two phase FGM plate.

Figure 3.2 shows the schematic diagram of the distribution patterns of carbon nanotubes in the plate under consideration. Cartesian coordinate system is taken into consideration and the variation of properties arise due to varying CNT distribution in the thickness coordinate. Static analysis is performed over a plate of $a \times b \times h$ dimensions in x,y,z directions respectively.

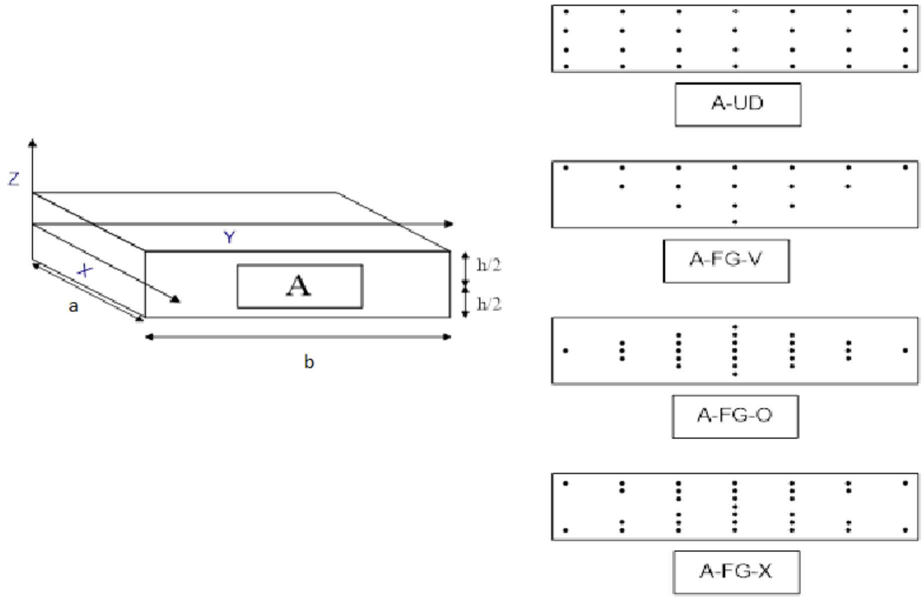

Figure 3.2 Distribution scheme and dimensions of the FGCNRTC plate.

3.2 Displacement Fields

The present work uses an inverse hyperbolic shear deformation theory (IHSDT) (Grover et al. 2013) to define the inplane (*u*,*v*) and transverse displacements (*w*). Mid-plane displacements (u_0, v_0, w_0) and shear rotations (θ_x, θ_y) are taken as the five field variables and displacements at a point on the plate is given by:

$$u(x,y,z) = u_0(x,y) - z\frac{\partial w_0}{\partial x} + \left(\sinh^{-1}\left(\frac{rz}{h}\right) - z\frac{2r}{h\sqrt{r^2+4}}\right)\theta_x$$

$$v(x,y,z) = v_0(x,y) - z\frac{\partial w_0}{\partial y} + \left(\sinh^{-1}\left(\frac{rz}{h}\right) - z\frac{2r}{h\sqrt{r^2+4}}\right)\theta_y$$

$$w(x,y,z) = w_0(x,y) \qquad \text{(3.1a-3.1c)}$$

Shear strain shape functions (coefficients of shear deformations) are chosen in such a manner that the displacements and stress distributions can be predicted realistically. Substituting $g(z) = \sinh^{-1}\left(\frac{rz}{h}\right)$ and $\Omega = z\frac{2r}{h\sqrt{r^2+4}}$ the given equations can be simplified as:

$$u(x,y,z) = u_0(x,y) - z\frac{\partial w_0}{\partial x} + (g(z) + \Omega z)\theta_x$$

$$v(x,y,z) = v_0(x,y) - z\frac{\partial w_0}{\partial y} + (g(z) + \Omega z)\theta_y$$

$$w(x,y,z) = w_0(x,y) \qquad \text{(3.2a-3.2c)}$$

where, Ω is a constant whose value is derived with the help of transverse shear stress boundary condition i.e. the shear stress disappears at the boundary and hence there is no need for a shear correction factor. The parameter r is the shear stress parameter whose value is taken equal to 3 (Grover *et al.*, 2013)

3.3 Strain-Displacement Relations

Since, the deformations and rotations are considered to be small, hence linear strain conditions can be applied. The strains $[\varepsilon_{xx}, \varepsilon_{yy}, \gamma_{xy}, \gamma_{xz}, \gamma_{yz}]$ under liner strain conditions are given by

$$\varepsilon_{xx} = \frac{\partial u}{\partial x} = \frac{\partial u_0}{\partial x} - z\frac{\partial^2 w_0}{\partial x^2} + (g(z) + \ \Omega \mathrm{z})\frac{\partial \theta_x}{\partial x}$$

$$\varepsilon_{yy} = \frac{\partial v}{\partial y} = \frac{\partial v_0}{\partial y} - z\frac{\partial^2 w_0}{\partial y^2} + (g(z) + \ \Omega \mathrm{z})\frac{\partial \theta_y}{\partial y}$$

$$\gamma_{xy} = \frac{\partial u}{\partial y} + \frac{\partial v}{\partial x} = \left(\frac{\partial u_0}{\partial y} + \frac{\partial v_0}{\partial x}\right) - z\frac{2\partial^2 w_0}{\partial x \partial y} + (g(z) + \ \Omega \mathrm{z})\left(\frac{\partial \theta_x}{\partial y} + \frac{\partial \theta_y}{\partial x}\right)$$

$$\gamma_{xz} = \frac{\partial u}{\partial z} + \frac{\partial w}{\partial x} = (g'(z) + \ \Omega)\theta_x$$

$$\gamma_{yz} = \frac{\partial v}{\partial z} + \frac{\partial w}{\partial y} = (g'(z) + \ \Omega)\theta_y$$

(3.3a-3.3e)

$\varepsilon_{xx}, \varepsilon_{yy}$ are normal strains in x and y directions respectively while γ_{xy} is the in plane shear strain and γ_{xz} are γ_{yz} are the transverse shear strains.

3.4 Constitutive Equations

Constitutive equations contains information about the behaviour of a structural element according to their material properties. It relates the stress developed in the structure for a given strain condition.

Generalised Hooke's law provides the relation between the stress tensor $\{\sigma\}_{5\times1}$ and the strain tensor $\{\varepsilon\}_{5\times1}$ and is given by the following relation.

$$\{\sigma\}_{5\times1} = [Q_{ij}]_{5\times5}\{\varepsilon\}_{5\times1} \tag{3.4a}$$

$$\begin{Bmatrix} \sigma_{xx} \\ \sigma_{yy} \\ \tau_{xy} \\ \tau_{yz} \\ \tau_{xz} \end{Bmatrix} = \begin{bmatrix} Q_{11} & Q_{12} & 0 & 0 & 0 \\ Q_{21} & Q_{22} & 0 & 0 & 0 \\ 0 & 0 & Q_{66} & 0 & 0 \\ 0 & 0 & 0 & Q_{44} & 0 \\ 0 & 0 & 0 & 0 & Q_{46} \end{bmatrix} \begin{Bmatrix} \varepsilon_{xx} \\ \epsilon_{yy} \\ \gamma_{xy} \\ \gamma_{yz} \\ \gamma_{xz} \end{Bmatrix} \tag{3.4b}$$

Where,

$$Q_{11} = \frac{E_{11}(z)}{1-\nu_{12}\nu_{21}} \ , \ Q_{22} = \frac{E_{22}(z)}{1-\nu_{12}\nu_{21}} \ , \ Q_{12} = \frac{\nu_{12}E_{11}(z)}{1-\nu_{12}\nu_{21}} \ ,$$

$$Q_{66} = G_{12}(z), \ \ Q_{44} = G_{23}(z), \ \ Q_{66} = G_{13}(z).$$

Where, $E_{11}(z), E_{22}(z)$, are the in plane Young's Moduli directions for the given functionally graded material and G_{12}, G_{12}, G_{12} are the shear moduli for the same. The value of these constants can be estimated for the case of functionally graded materials in different ways as discussed below. For the case of FGM with two isotropic phases $E_{11}(z) = E_{22}(z)$ and $G_{12}(z) = G_{23}(z) = G_{13}(z)$

3.4.1 Methods to predict effective material properties of functionally graded materials

Several methods exist in literature to predict the effective properties of composite materials. Some of the most common ones of those have been discussed here. Superscripts *c*, *m* signify ceramic phase and metal phase for the case of two phase FGM plates and CNT and matrix phases for the case of FGCNTRC plates.

(a) Rule of mixtures: Rule of mixtures is one of the easiest and most widely applied empirical relation to obtain properties of materials with two phases. According to this law longitudinal modulus (E_{11}), transverse modulus (E_{22}), shear modulus (G_{12}) of a composite material can be obtained by the following equations (Gibson 1994).

$$E_{11} = V_c E_{11}^c + V_m E^m$$

$$\frac{1}{E_{22}} = \frac{V_c}{E_{22}^c} + \frac{V_m}{E^m}$$

$$\frac{1}{G_{12}} = \frac{V_c}{G_{12}^c} + \frac{V_m}{G^m}$$

$$V_m + V_c = 1$$

(3.5a-3.5d)

Where, E^m, E_{11}^c are the longitudinal Young's modulus, E_{11}^c is the transverse modulus, G^m, G_{12}^c are the shear modulus and V_m, V_c are the volume fractions for the two phases under consideration.

(b) Mori Tanaka Scheme: Eshelby-Mori-Tanaka scheme is based an equivalent inclusion-average stress method. According to this scheme the equivalent stiffness tensor *C* of a composite made of a continuous matrix & *N-1* inhomogeneities is given by (Wanga and Pyrz, 2004)

$$\boldsymbol{C} = \boldsymbol{C_1} + \sum_{n=2}^{N} v_n \{(\boldsymbol{C_n} - \boldsymbol{C_1})\boldsymbol{T_n}\}[\sum_{n=1}^{N} v_n \boldsymbol{T_n}]^{-\mathbf{1}} \tag{3.6}$$

Here v_n represents the volume fraction of the n^{th} inhomogeneity and the curly brackets {} represent that an average over all possible orientations is taken into account. $\mathbf{T_n}$ represents the Wu tensor and is given by:

$$\boldsymbol{T_n} = \left[\boldsymbol{I} + \boldsymbol{S_n}\boldsymbol{C_1^{-1}}(\boldsymbol{C_r} - \boldsymbol{C_1})\right]^{-1} \tag{3.7}$$

$\mathbf{S_n}$ is the Elshelby Tensor and has different values for different shapes of impurities. One of the problems with Mori-Tanaka scheme is in the case of composites that are made up of isometric matrices reinforced with spheroidal transversely isotropic materials. In such composites the modulus calculated by the Mori-Tanka method might be outside the Hashin-Shtrikman-Walpole bounds, when high volume fractions of composites are considered (Walpole,1969).

(c) Extended Rule of mixture: Rule of mixture provides an empirical relationship for calculating the equivalent material properties of a composite but it does not consider factors like load efficiency of load transfer from reinforcement to matrix and vice-versa. This problem can be solved by using extended rule of mixture and it defines the value of equivalent moduli for the composite (Zhu *et al.* 2012)

$$E_{11} = \eta_1 V_c E_{11}^c + V_m E^m \tag{3.8a}$$

$$\frac{\eta_2}{E_{22}} = \frac{V_c}{E_{22}^c} + \frac{V_m}{E^m} \tag{3.8b}$$

$$\frac{\eta_3}{G_{12}} = \frac{V_c}{G_{12}^c} + \frac{V_m}{G^m} \tag{3.8c}$$

Where, E^m, G^m and V_m are the Yong's modulus and shear modulus and volume fraction of the matrix and V_c, E_{11}^c, G_{12}^c are the corresponding properties of reinforcements. The parameters η_1, η_2, η_3 are the efficiency parameters and are incorporated to account for the scale dependent material properties. Also the Poisson's ratio ν_{12} and the density ρ are expressed as

$$\rho = V_c\rho_{11}^c + V_m\rho^m$$
$$\nu_{12} = V_c^*\nu_{12}^c + V_m\nu^m$$
$$V_m + V_c = 1 \qquad \text{(3.9a-3.9c)}$$

3.4.2 Mathematical idealisation of functionally graded materials

Despite of being highly heterogeneous in composition FGMs are usually treated as a continua and their properties can be idealised by homogenisation schemes.

3.4.2.1 Functionally graded plates with two isotropic phases

a) **Power law:** The Power law assumes the variation of volume fraction of the ceramic materials at a given z coordinate $v_c(z)$ according to equation
$$v_c(z) = (z/h + 0.5)^N \qquad (3.10)$$
Where h is total thickness of the plate and *N* is the power law index. Substituting this value of ceramic volume fraction in the equation of rule of mixtures following relationship is obtained.
$$P_e = P_m + (P_c - P_m)v_c(z) \qquad (3.11)$$
where, *P (z)* is the effective material property (Young's modulus (*E*), shear modulus (*G*), Poisson's ratio (*v*) etc.) at any point in the material and P_c and P_m are the corresponding properties for the ceramic and the metal respectively. The value of different properties depend on the value of *N* which varies from *N*=0 (completely ceramic phase) to *N*=∞ (completely metal phase).

b) **Exponential Law:** In exponential law the variation of the volume fraction of ceramic phase is assumed according to an exponential function of thickness coordinate and the relation is given by
$$P_e = P_0 e^{N(z+0.5)} \qquad (3.12)$$
where, P_e is the effective property of the material at a certain value of *z* and P_0 is the property of the material at the bottom surface which in our case is metal so $P_0 = P_m$ in the given case. *N* is the exponential index on which the property of our material will depend.

3.4.2.2 Functionally graded carbon nanotube reinforced composite plates

In this method, different orientations of carbon nanotubes in the given matrix is considered. These are UD-CNTRC which has the uniform distribution of carbon nanotubes, and functionally graded distribution of carbon nanotubes namely FG-V, FG-O, FG-X CNTRC plates in which the carbon nanotubes are in the distributed in a functionally graded manner in the thickness direction. These distributions are shown in Figure 3.2

According to the manner in which the carbon nanotubes are distributed in the matrix the volume fraction of the carbon nanotubes is defined as

$$\begin{cases} V_c = V_c^* & (UD\ CNTRC) \\ V_c(z) = \left(1 + \frac{2z}{h}\right) V_c^* & (FG\text{-}V\ CNTRC) \\ V_c(z) = 2\left(1 - \frac{2|z|}{h}\right) V_c^* & (FG\text{-}O\ CNTRC) \\ V_c(z) = 2\left(\frac{2|z|}{h}\right) V_c^* & (FG\text{-}X\ CNTRC) \end{cases} \quad (3.13a\text{-}3.13d)$$

$$V_c^* = \frac{w_c}{w_c + \frac{\rho_c}{\rho_m} - \left(\frac{\rho_c}{\rho_m}\right) w_c} \quad (3.14)$$

w_c in the above equation represents the mass fraction of carbon nanotubes in the given composite. ρ_m and ρ_c are the densities of the matrix and the CNT respectively.

3.5. Analytical Solution for Static Analysis of Functionally Graded Composite Plate

The principle of virtual work are used to obtain the governing equations for the given IHSD theory. The principle of virtual work states that under equilibrium the sum of virtual work done by virtual forces is equal to zero for a system in equilibrium condition. It can be written as

$$\int_0^T (\delta U - \delta V) dt = 0 \quad (3.15)$$

Here $\delta U, \delta V$ are the virtual strain energy and the virtual work done by the applied forces respectively and are given by

$$\delta U = \int_{\Omega_0} \left\{ \int_{-h/2}^{h/2} \left(\sigma_{xx}\delta\varepsilon_{xx} + \sigma_{yy}\delta\varepsilon_{yy} + \tau_{xy}\delta\gamma_{xy} + \tau_{xz}\delta\gamma_{xz} + \tau_{yz}\delta\gamma_{yz} \right) dz \right\} dxdy \quad (3.16)$$

$$\delta V = \int_{\Omega_0} q\delta w_0 dxdy \quad (3.17)$$

Now we can derive the differential equations of Euler-Lagrange for static response under different loading conditions in terms of resultant stresses and moments by substituting $\delta U, \delta V$ in virtual work statement in equation (3.15). Then we substitute the values of virtual strains from equation (3.5) then integrating by parts to relieve it from any derivatives of generalised displacements. Using calculus of variations we obtain the following relations for a plate under the action of transverse load q, axial compression $N_{xx}$and N_{yy} and in-plane shear N_{xy} :

$$\frac{\partial N_{xx}}{\partial x} + \frac{\partial N_{xy}}{\partial y} = 0$$

$$\frac{\partial N_{xy}}{\partial x} + \frac{\partial N_{yy}}{\partial y} = 0$$

$$\frac{\partial^2 M_{xx}}{\partial x^2} + \frac{\partial M_{xy}}{\partial x \partial y} + \frac{\partial^2 M_{yy}}{\partial y^2} + q + \overline{N}_{xx}\frac{\partial^2 w_0}{\partial x^2} + 2\overline{N}_{xy}\frac{\partial^2 w_0}{\partial x \partial y} + \overline{N}_{yy}\frac{\partial^2 w_0}{\partial y^2} = 0$$

$$\Omega\frac{\partial M_{xx}}{\partial x} + \frac{\partial P_{xx}}{\partial x} + \Omega\frac{\partial M_{xy}}{\partial y} + \frac{\partial P_{xy}}{\partial y} - \Omega Q_1 - K_1 = 0$$

$$\Omega\frac{\partial M_{xy}}{\partial x} + \frac{\partial P_{xy}}{\partial x} + \Omega\frac{\partial M_{yy}}{\partial y} + \frac{\partial P_{yy}}{\partial y} - \Omega Q_2 - K_2 = 0$$

(3.18a-3.18e)

Where the resultant stresses and moments can be defined as:

$$\begin{bmatrix} N_{xx} & M_{xx} & P_{xx} \\ N_{yy} & M_{yy} & P_{yy} \\ N_{xy} & M_{xy} & P_{xy} \end{bmatrix} = \int_{\frac{-h}{2}}^{\frac{h}{2}} \begin{Bmatrix} \sigma_{xx} \\ \sigma_{yy} \\ \sigma_{xy} \end{Bmatrix} [1 \quad z \quad g(z)]dz$$

$$\begin{bmatrix} Q_2 & K_2 \\ Q_1 & K_1 \end{bmatrix} = \int_{\frac{-h}{2}}^{\frac{h}{2}} \begin{Bmatrix} \sigma_{yz} \\ \sigma_{xz} \end{Bmatrix} [1 \quad g'(z)]dz \qquad (3.19a\text{-}3.19b)$$

To obtain the governing equations in terms of field variables we apply the following integrals:

$$[A_{ij} \quad B_{ij} \quad D_{ij} \quad E_{ij} \quad F_{ij_{ij}} \quad H_{ij}] = \int_{\frac{-h}{2}}^{\frac{h}{2}} \left[Q_{ij}^{(k)}\right] \left[1 \quad z \quad z^2 \quad g(z) \quad z.g(z) \quad \left(g(z)\right)^2\right] dz$$

(3.20)

For $i, j = 1, 2, 3, 4, 5, 6$

$$[K_{ij} \quad L_{ij}] = \int_{\frac{-h}{2}}^{\frac{h}{2}} \left[Q_{ij}^{(k)}\right] \left[g'(z) \quad \left(g'(z)\right)^2\right] \qquad (i, j = 4,5) \qquad (3.21)$$

Substituting the values of above mentioned integrals in equations that we obtained by substituting values of resultant stresses and moments in equations (3.18) the following governing equations (Euler-Lagrange equations in displacement terms) are obtained:

$$
\begin{aligned}
&A_{11}\left(\frac{\partial^2 u_0}{\partial x^2}\right)+B_{11}\left(\Omega\frac{\partial^2\theta_x}{\partial x^2}-\frac{\partial^3 w_0}{\partial x^3}\right)+E_{11}\left(\frac{\partial^2\theta_x}{\partial x^2}\right)+A_{11}\left(\frac{\partial^2 v_0}{\partial x\partial y}\right)\\
&\quad+B_{12}\left(\Omega\frac{\partial^2\theta_y}{\partial x\partial y}-\frac{\partial^3 w_0}{\partial x\partial y^2}\right)+E_{12}\left(\frac{\partial^2\theta_y}{\partial x\partial y}\right)+A_{66}\left(\frac{\partial^2 u_0}{\partial y^2}+\frac{\partial^2 v_0}{\partial x\partial y}\right)\\
&\quad+B_{66}\left(\left(\Omega\frac{\partial^2\theta_x}{\partial y^2}+\frac{\partial^2\theta_y}{\partial x\partial y}\right)-2\frac{\partial^3 w_0}{\partial x\partial y^2}\right)+E_{66}\left(\frac{\partial^2\theta_x}{\partial y^2}+\frac{\partial^2\theta_y}{\partial x\partial y}\right)=0
\end{aligned}
$$

$$
\begin{aligned}
&A_{12}\left(\frac{\partial^2 u_0}{\partial x\partial y}\right)+B_{12}\left(\Omega\frac{\partial^2\theta_x}{\partial x\partial y}-\frac{\partial^3 w_0}{\partial x^2\partial y}\right)+E_{12}\left(\frac{\partial^2\theta_x}{\partial x\partial y}\right)+A_{22}\left(\frac{\partial^2 v_0}{\partial y^2}\right)\\
&\quad+B_{22}\left(\Omega\frac{\partial^2\theta_y}{\partial y^2}-\frac{\partial^3 w_0}{\partial y^3}\right)+E_{22}\left(\frac{\partial^2\theta_y}{\partial y^2}\right)+A_{66}\left(\frac{\partial^2 u_0}{\partial x\partial y}+\frac{\partial^2 v_0}{\partial x^2}\right)\\
&\quad+B_{66}\left(\left(\Omega\frac{\partial^2\theta_x}{\partial x\partial y}+\frac{\partial^2\theta_y}{\partial x^2}\right)-2\frac{\partial^3 w_0}{\partial x^2\partial y}\right)+E_{66}\left(\frac{\partial^2\theta_x}{\partial x\partial y}+\frac{\partial^2\theta_y}{\partial x^2}\right)=0
\end{aligned}
$$

$$
\begin{aligned}
&B_{11}\left(\frac{\partial^3 u_0}{\partial x^3}\right)+D_{11}\left(\Omega\frac{\partial^3\theta_x}{\partial x^3}-\frac{\partial^4 w_0}{\partial x^4}\right)+F_{11}\left(\frac{\partial^3\theta_x}{\partial x^3}\right)+B_{12}\left(\frac{\partial^3 v_0}{\partial x^2\partial y}+\frac{\partial^3 u_0}{\partial x\partial y^2}\right)\\
&\quad+D_{12}\left(\Omega\left(\frac{\partial^3\theta_y}{\partial x^2\partial y}+\frac{\partial^3\theta_x}{\partial x\partial y^2}\right)-2\frac{\partial^4 w_0}{\partial x^2\partial y^2}\right)+F_{12}\left(\frac{\partial^3\theta_y}{\partial x^2\partial y}+\frac{\partial^3\theta_x}{\partial x\partial y^2}\right)\\
&\quad+B_{22}\left(\frac{\partial^3 v_0}{\partial y^3}\right)+D_{22}\left(\Omega\frac{\partial^3\theta_y}{\partial y^3}-\frac{\partial^4 w_0}{\partial y^4}\right)+F_{22}\left(\frac{\partial^3\theta_y}{\partial y^3}\right)\\
&\quad+2B_{66}\left(\frac{\partial^3 u_0}{\partial x\partial y^2}+\frac{\partial^3 v_0}{\partial x^2\partial y}\right)+2D_{66}\left(\left(\Omega\frac{\partial^3\theta_x}{\partial x\partial y^2}+\frac{\partial^2\theta_y}{\partial x^2\partial y}\right)-2\frac{\partial^4 w_0}{\partial x^2\partial y^2}\right)\\
&\quad+2F_{66}\left(\frac{\partial^3\theta_x}{\partial x\partial y^2}+\frac{\partial^3\theta_y}{\partial x^2\partial y}\right)+q+\overline{N}_{xx}\frac{\partial^2 w_0}{\partial x^2}+\overline{2N}_{xy}\frac{\partial^2 w_0}{\partial x\partial y}+\overline{N}_{yy}\frac{\partial^2 w_0}{\partial y^2}=0
\end{aligned}
$$

$$
\begin{aligned}
&(\Omega B_{11}+E_{11})\left(\frac{\partial^2 u_0}{\partial x^2}\right)+(\Omega D_{11}+F_{11})\left(\Omega\frac{\partial^2\theta_x}{\partial x^2}-\frac{\partial^3 w_0}{\partial x^3}\right)+(\Omega F_{11}+H_{11})\left(\frac{\partial^2\theta_x}{\partial x^2}\right)\\
&\quad+(\Omega B_{12}+E_{12})\left(\frac{\partial^2 v_0}{\partial x\partial y}\right)+(\Omega D_{12}+F_{12})\left(\Omega\frac{\partial^2\theta_y}{\partial x\partial y}-\frac{\partial^3 w_0}{\partial x\partial y^2}\right)\\
&\quad+(\Omega F_{12}+H_{12})\left(\frac{\partial^2\theta_y}{\partial x\partial y}\right)+(\Omega B_{66}+E_{66})\left(\frac{\partial^2 u_0}{\partial y^2}+\frac{\partial^2 v_0}{\partial x\partial y}\right)\\
&\quad+(\Omega D_{66}+F_{66})\left(\left(\Omega\frac{\partial^2\theta_x}{\partial y^2}+\frac{\partial^2\theta_y}{\partial x\partial y}\right)-2\frac{\partial^3 w_0}{\partial x\partial y^2}\right)\\
&\quad+(\Omega F_{66}+H_{66})\left(\frac{\partial^2\theta_x}{\partial y^2}+\frac{\partial^2\theta_y}{\partial x\partial y}\right)-[\Omega^2 A_{55}+2\Omega K_{55}+L_{55}]\theta_x=0
\end{aligned}
$$

$$
\begin{aligned}
&(\Omega B_{12}+E_{12})\left(\frac{\partial^2 u_0}{\partial x\partial y}\right)+(\Omega D_{12}+F_{12})\left(\Omega\frac{\partial^2\theta_x}{\partial x\partial y}-\frac{\partial^3 w_0}{\partial x^2\partial y}\right)+(\Omega F_{12}+H_{12})\left(\frac{\partial^2\theta_x}{\partial x\partial y}\right)+\\
&(\Omega B_{22}+E_{22})\left(\frac{\partial^2 v_0}{\partial y^2}\right)+(\Omega D_{22}+F_{22})\left(\Omega\frac{\partial^2\theta_y}{\partial y^2}-\frac{\partial^3 w_0}{\partial y^3}\right)+(\Omega F_{22}+H_{22})\left(\frac{\partial^2\theta_y}{\partial y^2}\right)+\\
&(\Omega B_{66}+E_{66})\left(\frac{\partial^2 u_0}{\partial x\partial y}+\frac{\partial^2 v_0}{\partial x^2}\right)+(\Omega D_{66}+F_{66})\left(\left(\Omega\frac{\partial^2\theta_x}{\partial x\partial y}+\frac{\partial^2\theta_y}{\partial x^2}\right)-2\frac{\partial^3 w_0}{\partial x^2\partial y}\right)+\\
&(\Omega F_{66}+H_{66})\left(\frac{\partial^2\theta_x}{\partial x\partial y}+\frac{\partial^2\theta_y}{\partial x^2}\right)-[\Omega^2 A_{44}+2\Omega K_{44}+L_{44}]\theta_x=0
\end{aligned}
$$

(3.22a-3.22e)

Navier type closed form solutions are implied to find the displacement and stress for the given problems. It provides exact solution for the case where all the edges of the plate are simply supported. For a plate with dimensions ($a\times b\times h$) and all the edges simply supported the following boundary conditions are taken into account (SS1) (Reddy, 2004)

$$v_0=w_0=\theta_y=N_{xx}=M_{xx}=0\ \ at\ \ x=0 \text{ and } x=a$$

$$u_0=w_0=\theta_x=N_{yy}=M_{yy}=0\ \ at\ \ y=0 \text{ and } y=b$$

(3.23)

The mid plane displacements are assumed as described below:

$$u_0=\sum_{m=1}^{\infty}\sum_{n=1}^{\infty}U_{mn}\cos(\alpha x)\sin(\beta y)$$

$$v_0=\sum_{m=1}^{\infty}\sum_{n=1}^{\infty}V_{mn}\sin(\alpha x)\cos(\beta y)$$

$$w_0=\sum_{m=1}^{\infty}\sum_{n=1}^{\infty}W_{mn}\sin(\alpha x)\sin(\beta y)$$

$$\theta_x = \sum_{m=1}^{\infty}\sum_{n=1}^{\infty} X_{mn}\cos(\alpha x)\sin(\beta y)$$

$$\theta_y = \sum_{m=1}^{\infty}\sum_{n=1}^{\infty} Y_{mn}\cos(\alpha x)\sin(\beta y)$$

(3.24a-3.24e)

When we substitute the values of these field variables in the governing differential equations and simplify we obtain 5 simultaneous equations. These equations can be solved for the 5 unknowns (U_{mn}, V_{mn}, W_{mn}, X_{mn}, *and* Y_{mn}).

Static response: The plate is subjected to transverse load assumed in the form given in the equation (3.22) and hence all the other loads in equation (3.19c) will become zero. i.e. $\bar{N}_{xx}$= $\bar{N}_{yy}$= $\bar{N}_{xy}$= 0.

$$q = \sum_{m=1}^{\infty}\sum_{n=1}^{\infty} q_{mn}\sin(\alpha x)\sin(\beta y)$$

(3.25a)

Different values of q_{mn} are listed in Table 3.1.

Table 3.1 Fourier series expansion coefficients for different loading conditions in Navier method

Loading condition	Coefficient q_{mn}
Sinusoidal Load	$q_{mn} = q_0$
Uniformly Distributed Load	$q_{mn} = \dfrac{16q_0}{\pi^2 mn}$
Hydrostatic Load	$q_{mn} = (-1)^{n+1}\dfrac{8q_0}{\pi^2 mn}$
Central Point Load	$q_{mn} = \dfrac{4q_0}{ab}\sin\left(\dfrac{m\pi}{2}\right)\sin\left(\dfrac{n\pi}{2}\right)$

Simultaneous equations obtained by substituting the displacements in equation (3.22) and loads as given in Table 3.1 can be written in matrix form as

$$[\bar{R}]_{5\times5}\{\Delta\}_{5\times1} = \{q\}_{5\times1} \tag{3.25b}$$

Where $\{\Delta\}_{5\times1} = \{U_{mn}\ V_{mn}\ W_{mn}\ X_{mn}\ Y_{mn}\ \}^T$ and $\{q\}_{5\times1} = \{0\ 0\ q_{mn}\ 0\ 0\}^T$.

Mid-plane displacements can be found by substituting the values of $U_{mn}\ V_{mn}\ W_{mn}\ X_{mn}\ Y_{mn}$ obtained after solving the equation (3.25) for the value of Δ. To find the stresses we first substitute the values of mid plane displacements obtained in equation (3.25) into the strain displacement relations to obtain the strains then multiply the strains obtained with Q matrix.

3.6 Numerical Solution for Bending Analysis of Functionally Graded Plates

Exact solutions despite of their accuracy are very specific and it can be extremely difficult to use them in certain conditions. For example Navier solutions can only be applied to simply supported boundary conditions. For other boundary conditions, Levy solutions have to be used which are not easy to find out for every case. This problem is addressed with the help of Numerical methods. Finite element analysis (FEA) is one of the most common methodology to solve complex problems where finding exact solutions is not possible. Most of the commercial design and analysis software today use FEA to solve complex governing equations over complex domains. But finite element analysis and modelling use two different tools to define data sets, while in the modelling part NURBS geometries are used, finite element analyses uses polynomial to define shape function. Converting the geometry from a NURBS based data set to a shape function based data set is a time consuming process. Isogeometric analysis addresses this issue by applying same NURBS based shape functions for modelling and analysis.

3.6.1. Isogeometric analysis

As stated earlier isogeomatric analysis stakes its novelty on using same basis functions to define the geometry as well as for performing analysis on the object. NURBS basis functions are used for both designing and analysing the required parts. For the part of analyses the usual concepts of Finite Element Method (FEM) are retained in isogeometric analysis. For example Variational methods, equations of mechanics etc. are used for developing the governing equations and those equations are converted into linear form solvable by matrix algebra by applying the boundary and/or initial conditions.

3.6.2 B-Splines

B-splines are defined as a set piecewise polynomials that are continuous are differentiable in the given non-overlapping interval. Across the intervals the functions are continuous but not necessarily differentiable and the order of the continuity depends on the degree of the curve. These intervals are defined with the help of knot vectors. These piecewise functions can be used to define curves surfaces and 3-D geometries.

In B-splines the parameter space is defined over patches rather than over elements which is the case of finite element analysis. These patches can be made up of one or more individual elements defined according to the knot vectors. This differentiates the mapping in IGA from the mapping in FEA. These patches act as subdomains and can be very useful while modelling elements where properties change from one region to other such that each patch can be defined such that it has uniform properties. Each element in the physical space has a corresponding image in the parameter space but similar function (jacobian) is used for carrying out transformations between physical space and parametric space for all the element in a given patch.

3.6.3. Knot Vectors

Knot spans are used to define the notion of element in parametric space in isogeometric analysis i.e. knots divide the domain into patches and elements. Knot vector is a set of coordinates of the points connecting the subintervals and can be represented as

$$\Xi = [\xi_1, \xi_2, \xi_3 \ \dots \ \xi_{n+p+1}] \tag{3.26}$$

Where ξ_i is the ith knot, *p* is the degree of the polynomial and *n* is the total number of control points. ξ_i to ξ_{i+1} represents a knot span. In a knot span the basis function is C^{∞} continuous while at the the knot junctions it is C^{p-m} continuous where *p* is the degree of the curve and m is the number of times a knot is repeated. Hence it is evident that multiple knot vectors at a point reduces the continuity of the curve. A knot vector where the first and last knot vectors are repeated *p+1* times then it is called an open knot vector. Open knot vector facilitates the interpolation of the curve between two elements.

3.6.4. Basis Functions

B-spline basis functions are defined by the Cox-de Boor recursion formula and it is given by equation for the value of *p=0*.

$$N_{i,0}(\xi) = \begin{cases} 1 & \text{if } \xi_i \le \xi < \xi_{i+1} \\ 0 & \text{otherwise} \end{cases} \tag{3.27a}$$

For higher values of *p* the formula is written as given in equation (3.27b)

$$N_{i,p}(\xi) = \frac{\xi - \xi_i}{\xi_{i+p} - \xi_i} N_{i,p-1}(\xi) + \frac{\xi_{i+p+1} - \xi}{\xi_{i+p+1} - \xi_{i+1}} N_{i+1,p-1}(\xi)$$

(3.27b)

Figure shows the variation of quadratic basis functions over the domain for knot vector of $\Xi =$ [0 0 0 0.25 0.50 0.75 1 1 1]. It can be seen that the effect of different basis vector varies for different knot spans or elements.

Derivatives of B-splines are necessary for the numeric analysis of the FGM plates. Derive of a function with degree *p* and *n* number of control points for a knot vector Ξ is given by

$$\frac{d}{dx} N_{i,p}(\xi) = \frac{p}{\xi_{i+p} - \xi_i} N_{i,p-1}(\xi) - \frac{p}{\xi_{i+p+1} - \xi_{i+1}} N_{i+1,p-1}(\xi)$$

(3.28)

3.6.5. B-Spline Curves

B-spline curves are simplest geometry that can be built by a B-splines basis function. It is a linear combination of different B-spline basis functions multiplied by their respective control points as coefficients. A B-spline curve for a given degree and set of control points is defined by the following equations

$$C(\xi) = \sum_{i=1}^{n} N_{i,p}(\xi) B_i$$

(3.29)

Where, $N_{i,p}(\xi)$ is the value of B-spline basis function and B_i is the corresponding control point.

3.6.6. B-spline Surface

In case of 2-D geometry B-splines basis functions can be used to describe surfaces. If $\Xi = [\xi_1 \quad \xi_2 \quad \xi_3 \cdots \quad \xi_{n+p+1}]$ and $\Psi = [\eta_1 \quad \eta_2 \quad \eta_3 \cdots \quad \eta_{n+p+1}]$ are the knot vectors in ξ and η directions respectively. Then two set of B-splines basis functions $N_{i,p}(\xi)$, $M_{j,q}(\eta)$ in perpendicular directions with degrees p and q respectively can be multiplied to form the equation for B-splines surfaces and the resulting equation will be represented as

$$S(\xi,\eta) = \sum_{i=1}^{n} N_{i,p}(\xi) M_{i,q} B_{i,j} \tag{3.30}$$

Where $B_{i,j}$ is the control point corresponding to the shape function $N_{i,p}$.

3.6.7. Non Uniform Rational B-Spline

Non uniform rational B-splines are used a basis function in IGA to represent the variation of variable over the domain. NURBS can understood to be made up for different piecewise B-splines functions rationalised with the help of constant weights and the value of the function at a point is derived by dividing the function value with the sum of all basis function at a point multiplied by their respective weights as shown in the following equation.

$$W(\xi) = \sum_{i=1}^{n} N_{i,p}(\xi) w_i \tag{3.31}$$

Where w_i are weights corresponding to a basis function $N_{i,p}(\xi)$ and $W(\xi)$ is dividing constant for a given point in the domain.

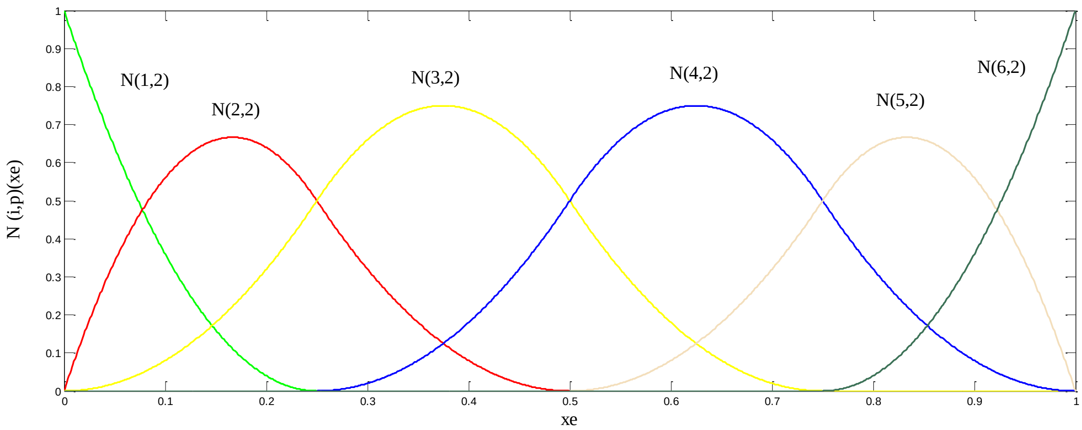

Figure 3.3 Basis functions for a quadric curve for a knot vector $\Xi =$ [0 0 0 0.25 0.50 0.75 1 1 1].

Usability of NURBS is aided by the fact that they can easily define any shape by just selecting a different value of the set of weights. Other than the above mentioned points NURBS inherit all the properties of the B-splines i.e. by a basis function can be modified according to our requirement by choosing different value of order, number of control points weights etc.

NURBS basis function are given by following equation

$$R_{i,p}(\xi) = \frac{N_{i,p}(\xi)w_i}{W(\xi)} = \frac{N_{i,p}(\xi)w_i}{\sum_{i=1}^{n} N_{i,p}(\xi)w_i}$$

(3.32)

NURBS basis functions in two dimensions are obtained by multiplying the basis functions in the two directions. These functions are used as the basis functions in the FEA formulation that proceeds. The following equation is used to find the basis function $R_{i,j}^{p,q}(\xi,\eta)$.

$$R_{i,j}^{p,q}(\xi,\eta) = \frac{N_{i,p}(\xi)M_{j,q}(\eta)w_{i,j}}{\sum_{i=1}^{n}\sum_{j=1}^{m} N_{i,p}(\xi)M_{j,q}(\eta)w_{i,j}}$$

(3.33)

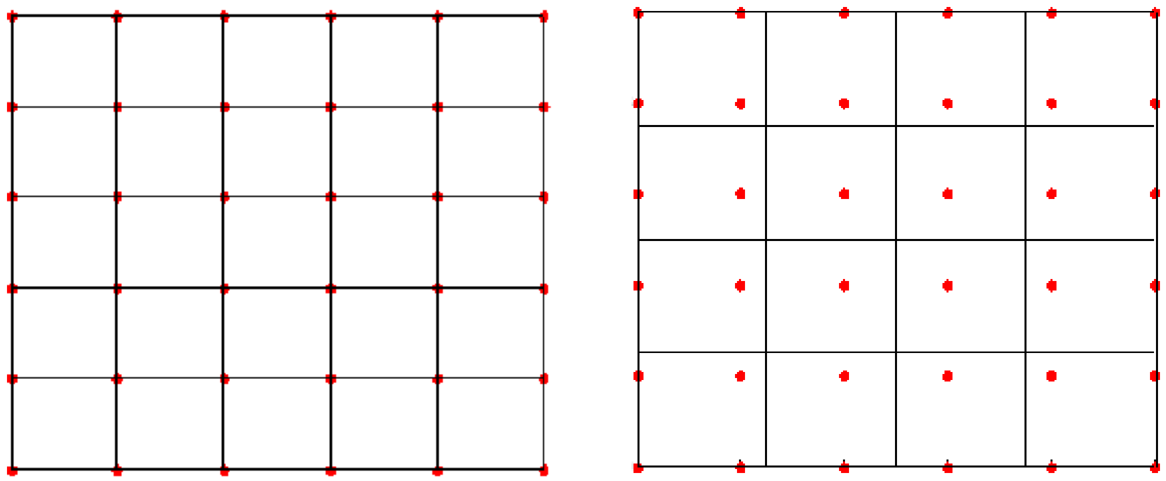

a b

Figure 3.4 Control points and elements for NURBS (a) *p*=1 (b) *p*=2.

Where, $N_{i,p}(\xi)$ and$M_{j,q}(\eta)$ are the shape functions in ξ and η directions respectively, while $w_{i,j}$ is the weight corresponding to a given point.

The derivatives of the NURBS basis function are required to formulate the stiffness matrix in the FEA analysis and derivative of a NURBS basis function is defined as

$$\frac{d}{dx}R_{i,p}(\xi) = w_i \frac{W(\xi)N'_{i,p}(\xi) - W'(\xi)N_{i,p}(\xi)}{(W(\xi))^2}$$

(3.34)

here, superscript ' corresponds to the derivative of that quantity. The derivative of the denominator can be found with the help of the following equation

$$W'(\xi) = \sum_{i=1}^{n} N'_{i,p}(\xi)w_i$$

(3.35)

3.6.8. Spaces and Mappings

In finite element analysis we deal with physical space defined by different nodal values and a parent element where the Gaussian integration takes place. Jacobians are used to traverse between physical space and parent element and vice versa when the integration is done. Similar to FE analysis there are different spaces to facilitate Gaussian integration.

(a) Physical Space: Actual NURBS geometry which is a linear combination of basis functions and control points is represented in the physical space. Physical mesh is the combination of the elements which are represented with the help of patches or knot spans. In the given analysis the knot spans are assumed as elements. Knots are points in 1-D, curves in 2-D and surfaces in 3-D.

(b) Control Mesh: Control mesh is formed by interpolating the control points in the physical space. It is used to control the shape of the geometry being formed by NURBS basis functions. The B-splines based curves and geometries have the convex hull property, which states that a B-splines curve can never cross the boundary formed by the control mesh. A control mesh can be formed by connecting the asterisks in Figure 3.4. It can also be observed from the Figure that changing degree of the B-splines has no effect on the control mesh.

(c) Parametric Space: The space where the NURBS basis functions $R_{i,p}(\xi)$ are defined is called the parametric space. For the sake of simplicity, the present analyses the area of the parametric space is taken as [0 1]×[0 1]. Every element in parametric space is mapped into the physical space.

(d) Parent element: Parent element is space which is utilised to make use of Gaussian quadrature for integration. It has a constant area of [-1,1]×[-1,1]. We map the element from parametric space into the parent element to perform integration. Following relations are used for this mapping the element from parent element $(\hat{\xi}, \hat{\eta})$ into parametric space (ξ, η)

$$\xi(\hat{\xi}) = \frac{(\xi_{i+1} - \xi_i)\hat{\xi} + (\xi_{i+1} + \xi_i)}{2}$$

$$\eta(\hat{\eta}) = \frac{(\eta_{i+1} - \eta_i)\hat{\eta} + (\eta_{i+1} + \eta_i)}{2}$$

(3.36a-3.36b)

3.6.9. Degree of freedom at a given control point

For the given displacement field the minimum continuity requirement is C^1 but formulating with C^1 continuity leads to increased computational cost and results couldn't be obtained for NURBS basis function with degree 1. The C^1 continuity formulation can be obtained with 5 degree of freedom per node. In the present analysis a C^0 continuous formulation is developed by introducing two extra degrees of freedoms making the total degrees of freedom per node equal to 7. The two extra degrees of freedom $\emptyset_x, \emptyset_y$ are defined as

$$\frac{\partial w_0}{\partial x} - \emptyset_x = 0$$

$$\frac{\partial w_0}{\partial y} - \emptyset_y = 0$$

(3.37a-3.37b)

3.6.10 Strain energy due to linear strains

Strain energy corresponding to linear strains obtained via equation (3.3) is to formulate the governing equations. Generalised strains are obtained according to degree of freedom

$$\{\varepsilon_L\}_{5\times1} = [H]_{5\times13}\{\bar{\varepsilon}\}_{13\times1} \tag{3.38}$$

Writing the generalised strains in the form of field variables we get

$$\{\bar{\varepsilon}_L\}_{13\times1} = [L]_{13\times7}\{q_i\}_{7\times1} \tag{3.39}$$

Where, $\{q_i\}_{7\times1} = \left[u_0, v_0, w_0, \theta_x, \theta_y, \emptyset_x, \emptyset_y\right]^T$

Substituting the value of basis functions and their derivatives from equations (3.33-3.34) in equation (3.39) we can obtain the value of element stiffness matrix.

$$\{\bar{\varepsilon}_L\}_j = [B]_j\{q_i\}_j \tag{3.40}$$

The strain energy for the j^{th} element can be derived in following manner

$$U_l^{(j)} = \frac{1}{2}\int_v \{\varepsilon_L\}_j^T\{\sigma\}\,dv = \frac{1}{2}\int_v \{\varepsilon_L\}_j^T\left[Q_{i,j}\right]\{\varepsilon_L\}_j dv = \frac{1}{2}\int_v \{\overline{\varepsilon_L}\}_j^T[H]_j^T\left[Q_{i,j}\right][H]_j\{\overline{\varepsilon_L}\}_j dv$$
$$= \frac{1}{2}\int_s \{q\}_j^T[B]_j^T[D]\,[B]_j\{q\}_j dxdy = \frac{1}{2}\{q\}_j^T[K_j]\{q\}_j \tag{3.41}$$

Using the elemental K_j matrix obtained from the above calculations for every element the value of global stiffness matrix *[K]* can be obtained.

$$U = \sum_{j=1}^{nel} U_j = \frac{1}{2}\{q\}^T[K]\{q\} \tag{3.42}$$

3.6.11. Work done by external forces

Work done due to the external forces W can be used to give the force matrix in the final formulation. It can be written in the form of field variables as follows.

$$W = \sum_{j=1}^{nel} W_j^{(e)} = \sum_{j=1}^{nel}\int_{A_j^{(e)}} p(x,y)w dA_j^{(e)} = \sum_{j=1}^{nel}\left\{f^{(e)}\right\}_j\{q\}_j = \{F\}\{q\} \tag{3.43}$$

Where, $\{f\} = [0\ 0\ p_0\ 0\ \ 0\ 0\ 0]$ and the value of p_0 can be found according to the loading condition from Table 3.1.

3.6.12. Derivation of governing equations

Governing equation for the given formulations are obtained by the help of the above derived energy terms and Lagrange equation for a conservative system which can be written as

$$\frac{d}{dt}\left(\frac{\partial L}{\partial \dot{\ell}_i}\right) - \frac{dL}{d\ell_i} = 0$$

(3.44)

Where, L is defined as the Lagrange constant and can be calculated from potential energy T and kinetic energy $V\ as\ L = T - W$. Substituting the values of potential and kinetic energies in the Lagange equations following governing equations can be obtained in matrix form.

$$[K]\{q\} = \{F\} \qquad (3.45)$$

Solving equation (3.45) for q we get the value of plate deflection at different points and in different directions.

3.6.13. Boundary conditions

For further analysis simply supported and clamped boundary conditions are taken into consideration. Constraints on the degrees of freedoms for a particular node on a given edge are applied as follows:

Clamped boundary conditions:

$$u_0 = v_0 = w_0 = \theta_x = \theta_y = N_{xx} = N_{yy} = M_{xx} = M_{yy} = 0 \text{ at all the edges} \qquad (3.46)$$

Simply supported boundary conditions:

$$v_0 = w_0 = \theta_y = N_{xx} = M_{xx} = 0\ \ at\ \ x = 0 \text{ and } x = a$$

$$u_0 = w_0 = \theta_x = N_{yy} = M_{yy} = 0\ \ at\ \ y = 0 \text{ and } y = b \qquad (3.47)$$

3.7 Summary

The governing equations required to obtain the bending behaviour of a FGM plate under different loading and boundary conditions are developed. Solution methodology is given both for the case of closed form Navier solution and isogeomatric framework. Both the cases take into account same displacement fields from the inverse hyperbolic shear deformation theory. In the case of IGA, Lagrange equations are used to find out the governing equations and in the case of analytical solutions, principle of virtual work is used.

Chapter 4

Results and Discussion

4.1 Introduction

In this chapter various numerical examples are considered in order to assess the applicability of the present methods developed both in terms of physical modelling and solution methodology. Analysis is carried out for two kinds of FGM plates: (1) For FGM plates with two isotropic phases (2) for functionally graded carbon nanotube reinforced plates. The obtained results are compared with those available in literature to approve their validity. The effect of different parameters like the span to thickness ratio, aspect ratio, power law index, Volume fraction of CNT and distribution of CNT is considered.

4.2 Analyses of FGM Plate with Two Isotropic Phases via Closed Form Solutions

A simply supported plate composed of aluminium and alumina (Al_2O_3) as the metal and ceramic parts is considered for this simulation. The mechanical properties the constituents of this plate are: E_m (Young's modulus for metal) = 70 GPa, E_c (Young's modulus for ceramic) = 380 GPa. The Poisson's ratio is assumed to be 0.3 for both the ceramic and metal. For the static analysis the non-dimensional displacement, shear and normal stress are evaluated. Different loading conditions are also taken into account.

The following non-dimensionalities are used in this formulation:

$$\bar{w} = \frac{10E_c h^3}{q_0 a^4} w\left(\frac{a}{2}, \frac{b}{2}\right)$$

$$\bar{\sigma}_{xx} = \frac{h}{q_0 a} \bar{\sigma}_{xx}\left(\frac{a}{2}, \frac{b}{2}, z\right)$$

$$\bar{\tau}_{xy} = \frac{h}{q_0 a} \bar{\tau}_{xy}\left(\frac{a}{2}, \frac{b}{2}, z\right)$$

(4.1a-4.1c)

where, $\bar{w}$, $\bar{\sigma}_{xx}$, $\bar{\tau}_{xy}$ are the non-dimensional transverse displacement, normal stress and shear stress respectively.

The validation of the present theory is done by comparing the displacement and stress values obtained with the help if IHSDT along with results due to various shear deformation theories available in literature and is depicted in Table 4.1.

Table 4.1 Validation of non-dimensional stresses and displacement for a square plate with *a/h*=10

N	Theory	$\bar{w}$	$\bar{\sigma}_{xx}$	$\bar{\tau}_{xy}$
1	SSDT Zenkour (2006)	0.5889	1.4894	0.611
	Quasi-3-D Carrera *et al.* (2008)	0.5875	1.5062	0.6081
	TSDT Wu and Li (2010)	0.589	1.4898	0.6111
	Quasi-3-D Wu and Chiu (2011)	0.5876	1.5061	0.6112
	HSDT Mantari *et al.* (2012)	0.588	1.4888	0.6109
	HSDT Thai and Kim (2013)	0.589	1.4898	0.6111
	HSDT Kulkarni *et al.* (2015)	0.5884	1.4891	0.611
	Present	0.5883	1.4892	0.611
2	SSDT Zenkour (2006)	0.7573	1.3954	0.5441
	Quasi-3-D Carrera *et al.* (2008)	0.757	1.4147	0.5421
	TSDT Wu and Li (2010)	0.7573	1.396	0.5442
	Quasi-3-D Wu and Chiu (2011)	0.7571	1.4133	0.5436
	HSDT Mantari *et al.* (2012)	0.7564	1.394	0.5438
	HSDT Thai and Kim (2013)	0.7573	1.396	0.5442
	HSDT Kulkarni *et al.* (2015)	0.7569	1.3946	0.5439
	Present	0.7567	1.3947	0.5439
4	SSDT Zenkour (2006)	0.8819	1.1783	0.5667
	Quasi-3-D Carrera *et al.* (2008)	0.8823	1.1985	0.5666
	TSDT Wu and Li (2010)	0.8815	1.1794	0.5669
	Quasi-3-D Wu and Chiu (2011)	0.8823	1.1841	0.5671
	HSDT Mantari *et al.* (2012)	0.8814	1.1755	0.5662
	HSDT Thai and Kim (2013)	0.8815	1.1794	0.5669
	HSDT Kulkarni *et al.* (2015)	0.882	1.1766	0.5664
	Present	0.8818	1.1766	0.5664
8	SSDT Zenkour (2006)	0.975	0.9466	0.5856
	Quasi-3-D Carrera *et al.* (2008)	0.9738	0.9687	0.5879
	TSDT Wu and Li (2010)	0.9747	0.9477	0.5858
	Quasi-3-D Wu and Chiu (2011)	0.9739	0.9622	0.5883
	HSDT Mantari *et al.* (2012)	0.9737	0.9431	0.585
	HSDT Thai and Kim (2013)	0.9746	0.9477	0.5858
	HSDT Kulkarni *et al.* (2015)	0.9747	0.9447	0.5853
	Present	0.9744	0.9444	0.5852

The span to thickness ratio is considered to be 10 and the FGP considered here is square. The values of power law index *N* is taken to be 1,2,4,8. The plate is subjected to a sinusoidal load. The results are validated by comparing them with the results obtained by Zenkour (2006), Carrera *et al.* (2008), Wu and Li (2010), Wu and Chiu (2011), Mantari *et al.* (2012), Thai and Kim (2013) and Kulkarni *et al.* (2015).

Further an exponentially graded plate is considered for the static analysis and the non-dimensional deflection is obtained for the plate with a simply supported loading condition. Table 4.2 provides verification of the IHSDT for different values of exponential law index. It can be seen that the values obtained from the current analysis are in close agreement with those available in literature. It can also be observed that the difference in values of deflection obtained by IHSDT and those of quasi 3-D increases with an increase in the value of power law index.

Table 4.2 Validation of non-dimensional transverse deflection for FGM plate with *a/h*=10 for FGM plate with exponential variation of properties

a/b	Theory	*N*=0.1	*N*=0.3	*N*=0.5	*N*=1	*N*=1.5
1	Quasi 3-D Mantari and Soares (2012)	0.2799	0.2531	0.2287	0.1772	0.1370
	Present	0.2813	0.2546	0.2306	0.1805	0.1416
2	Quasi 3-D Mantari and Soares (2012)	0.7037	0.6364	0.5752	0.4457	0.3445
	Present	0.7061	0.6401	0.5814	0.4610	0.3700
3	Quasi 3-D Mantari and Soares (2012)	0.8788	0.8027	0.7255	0.5662	0.4346
	Present	0.8904	0.8075	0.7341	0.5844	0.4724

Figure 4.1 shows the variation of normal stress $\bar{\sigma}_{xx}(a/2,b/2,z)$ with non-dimensional thickness *z/h* for a simply supported plate is subjected to sinusoidal load. It can be seen from the graph that the value of tensile stress is maximum at the top surface of the plate and increases with increase in the power law index. The maximum compressive stress does not shows the same behaviour and its value is maximum for the case of an isotropic plate i.e. *N*=0. The value of maximum compressive stress may not be at the bottom surface, for the case of plates with a lower power law index.

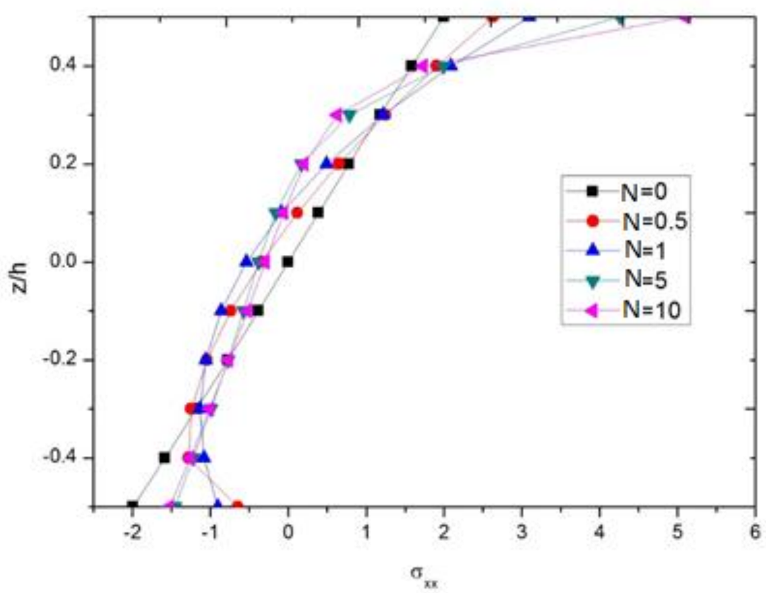

Figure 4.1 Variation of normal stress with non-dimensional thickness for a functionally graded plate with *a/h*=10 under sinusoidal loading

The variation of non-dimensional displacement with the span to thickness ratio of a simply supported is presented in Figure 4.2. The deflection is considered for SSL and UDL loading for *N*=1. It is observed from the figure, that the value of non-dimensional displacement increases with increase in span to thickness ratio. The difference is more in the initial stages but decrease more gradually after a certain value of span ratio is reached. Moreover the deflection of the plate under UDL is more than that of plate subjected to SSL.

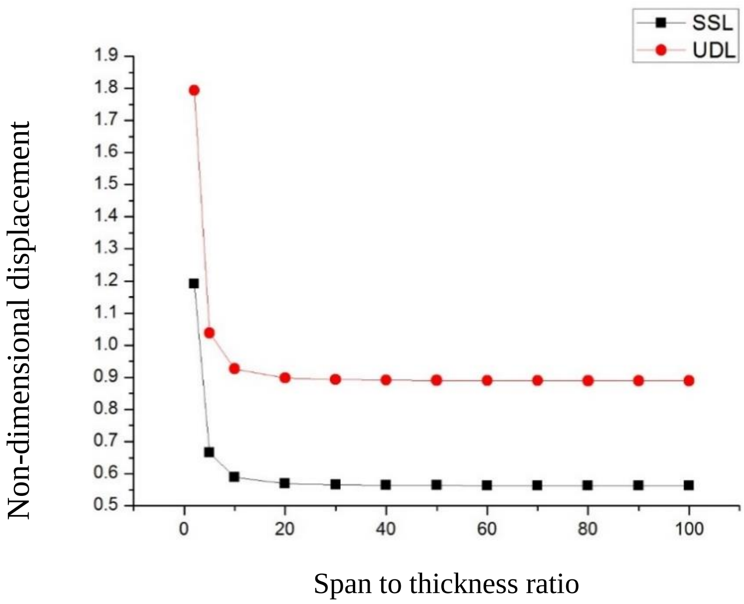

Figure 4.2 Variation of non-dimensional displacement with span ratio for SSL and UDL loading and *N*=1

Figure 4.3 shows the variation of non-dimensional transverse displacement with power law index. It is depicted in the figure that the transverse displacement increases as the value of power law index increases. It is understandable as we increase the value of power law index the properties of plate reach towards the properties of metals. Moreover a thin plate possess lower non-dimensional deflection relative to thick plate for a specific power law index.

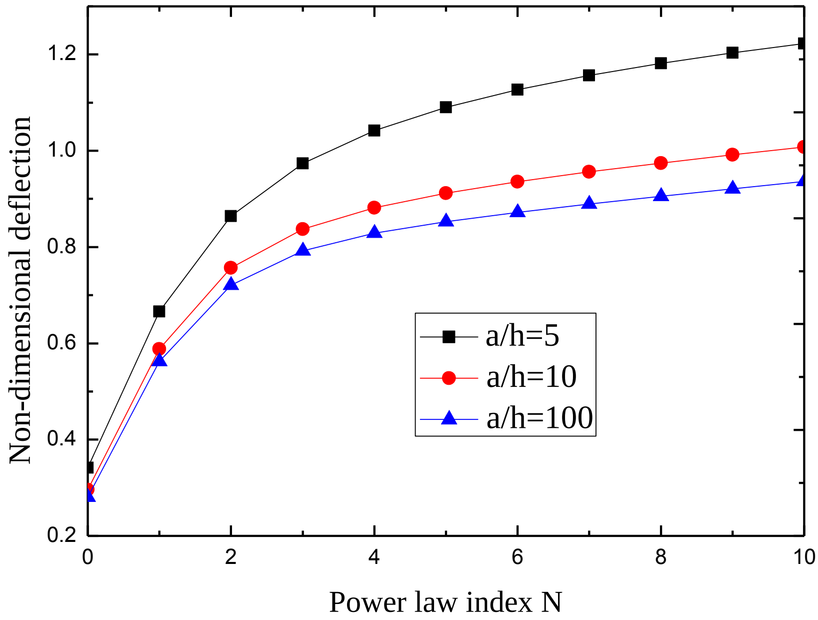

Figure 4.3. Variation of non-dimensional transverse displacement with the power law index under sinusoidal loading

Figure 4.4 shows the distribution of transverse shear stress along the thickness coordinate for a functionally graded plate with *a/h*=10 under sinusoidal loading conditions. The material property distribution is idealised by the help of power law. The results are plotted for different values of the power law index. Figure 4.4 depicts that the value of transverse shear stress is maximum near the mid plane and is equal to zero at the top and bottom surfaces, hence verifying the authenticity of shear strain coefficient in IHSDT.

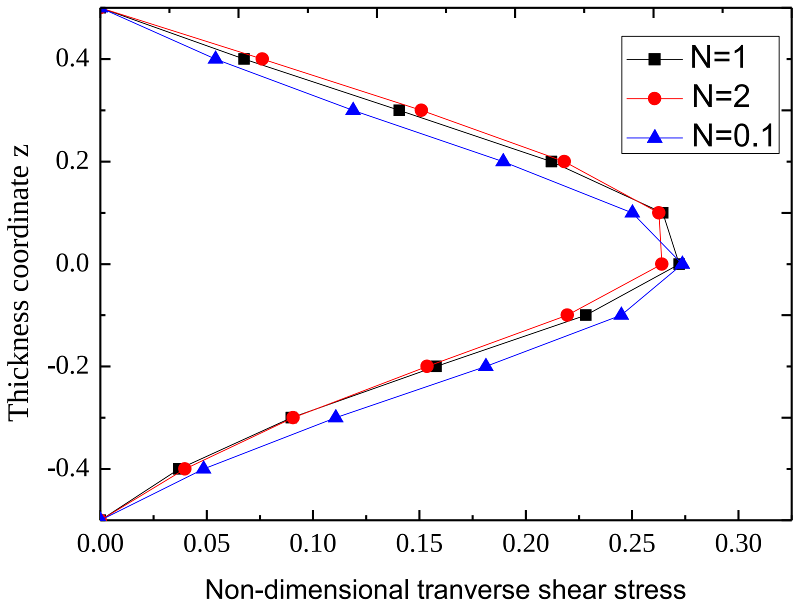

Figure 4.4 Variation of non-dimensional transverse shear stress along the thickness direction for simply supported FGM plate under sinusoidal loading.

4.3 Analyses of FGM Plate with Two Isotropic Phases via Isogeometric Analysis (IGA)

The following section deals with the isogoemetric analysis of functionally graded plates under different boundary conditions and different loading conditions. An Al/Al_2O_3 plate is analysed and results are generated for the effect of span to thickness ratio, the degree of curve and power law index on deflection values and convergence.

4.3.1. Convergence study

Figure 4.5 shows the variation of non-dimensional deflection with the number of control points per edge for a plate with CCCC boundary condition for a square FGM plate. Uniformly distributed transverse load is acting on the plate. The curve is drawn for values of deflection using formulation with one and two degree B-splines basis functions. From the Figure it is evident that the value of deflection converges faster when $p=2$. Material properties vary according to the power law with $N=1$.

Figure 4.6 demonstrates the effect of span to thickness ratio on the convergence rate in isogeometric analysis of FGM plates. The curves are plotted for the variation of deflection with number of control points per edge of the plate.

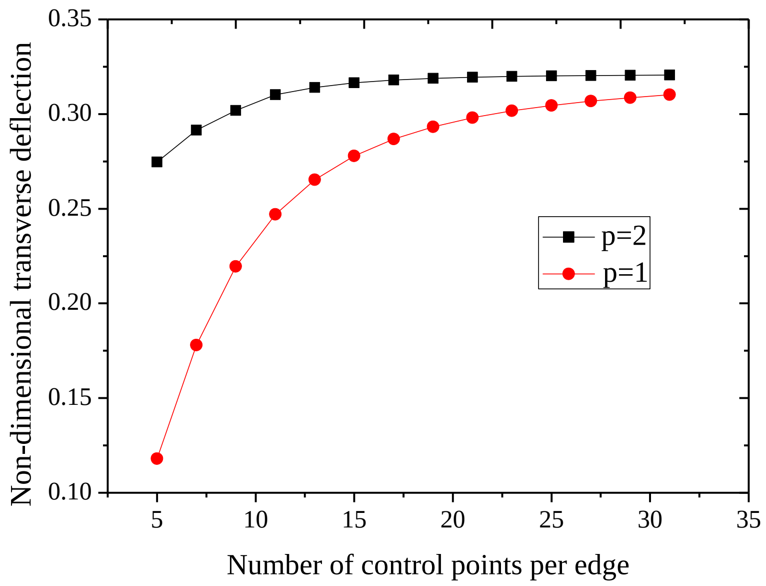

Figure 4.5 Effect of degree of basis function on the rate of convergence for a functionally graded plate with N=1.

A square plate with simply supported boundary conditions is taken into consideration. The degree of the curves and power law index are set equal to 1. Two values of span to thickness ratio are taken into account, *a/h=5* and *a/h=10*. It is observed from the figure that the results for thick plates converge faster than those for thinner plate.

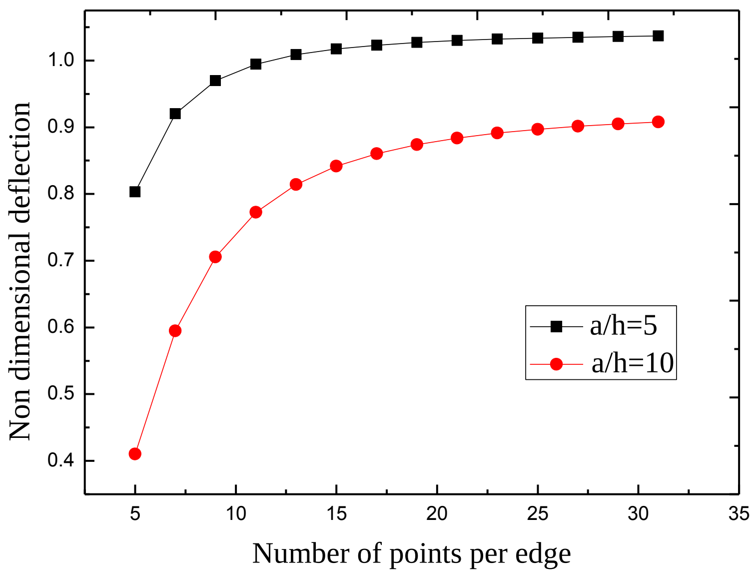

Figure 4.6 Effect of span to thickness ratio on the rate of convergence for IGA with basis functions of degree p=1.

Figure 4.7 shows the variation of non-dimensional deflection with number of elements per edge for different values of power law index. The bending behaviour of a square FGM plate with clamped boundary conditions is studied for a uniformly distributed load and the value of span to thickness ratio is taken as 20. It is concluded from the Figure that convergence is faster for FGM plates with lower power index.

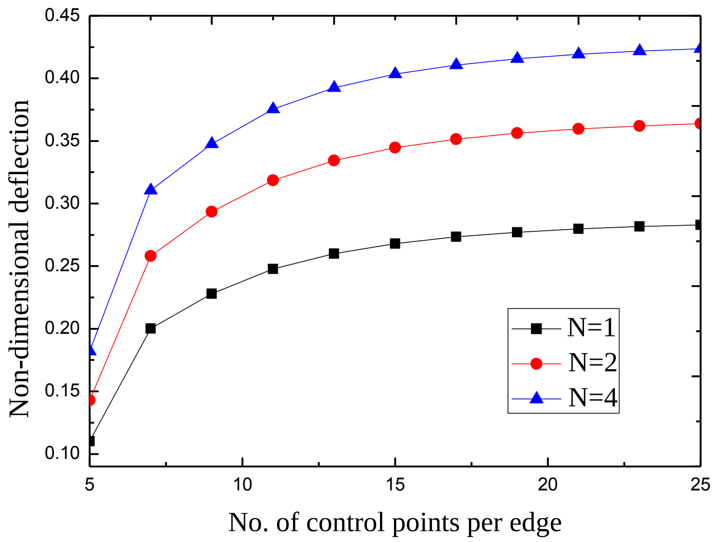

Figure 4.7 Effect of power law index *N* on the convergence rate for the IGA analyses of a FGM plate with *a/h*=20.

4.3.2. Validation of bending analysis results obtained using IGA

Table 4.3 lists the value of deflection for different values of the power law index *N* and under different support conditions (SSSS, CCCC, CSCS). A square FGM plate with gradation according to the power law is considered in this example. The sinusoidal loading conditions are considered here for *a/h*=5, 10. Analyses is performed using degree one B-splines for formulation. From the table it is clear that the results are in close agreement hence validating the use of IGA for bending analyses of FGM plates.

Table 4.3. Non-dimensional deflection for IGA analysis of FGCNTR composite square plates with *p*=1

a/h	*N*	Theory	SSSS	CCCC	CSCS
5	1	Analytical solution	1.0382	-	-
		IGA	1.0367	0.4417	0.6214
	2	Analytical solution	1.3434	-	-
		IGA	1.3427	0.5798	0.8133
	4	Analytical solution	1.6129	-	-
		IGA	1.6097	0.7313	1.0133
	8	Analytical solution	1.8290	-	-
		IGA	1.8222	0.8616	1.1820
10	1	Analytical solution	0.9264	-	-
		IGA	0.9187	0.3201	0.4726
	2	Analytical solution	1.1897	-	-
		IGA	1.1811	0.4140	0.6103
	4	Analytical solution	1.3849	-	-
		IGA	1.3759	0.4938	0.7237
	8	Analytical solution	1.5307	-	-
		IGA	1.5183	0.5567	0.8119

4.4. Analysis of FGCNTRC Plates using Closed Form Solutions

The static analysis of a FGCNTRC plate is performed under different loading conditions using Navier's solutions for the case of simply supported square plate. Poly{(m-phenylenevinylene)-co-[(2,5-dioctoxy-p-phenylene) vinylene]} or PmPV (Han and Elliot 2007) is used as the matrix material and its material properties are taken as $E^m = 2.1$ GPa, $\nu^m = 0.34$ GPa. The shear modulus can be calculated using $G^m = E^m/2(1+\nu^m)$. Single Walled Carbon Nanotubes with arm chair configuration (chirality angle = 30^0) are used in this study. The material properties of the CNT are listed by using MD simulations results of Zang and Shen (2006) and are given by: $E_{11}^c = 5.6466$ TPa, $E_{22}^c = 7.0800$ TPa, $G_{12}^c = 1.9445$ TPa, $\nu_{12}^c = 0.175$. The values of the efficiency factors are mentioned in Table 4.4 and their values are calculated by comparing the values of coefficients obtained from molecular dynamics simulations with those obtained by the rule of mixtures. Effective properties of the CNTRC plate are calculated by substituting the values of the properties in the extended rule of mixture. In addition to the above mentioned parameters, we take $G_{12} = G_{13} = G_{23}$.

Table 4.4 Efficiency parameters of SWCNT

Volume fraction of CNT (V_c^*)	η_1	η_2	η_3
0.11	0.149	0.943	0.943
0.14	0.150	0.941	0.941
0.17	0.149	1.381	1.381

Different numerical examples are considered to study the bending behaviour of the given plate. A square plate (*a/b=1*) with span ratios (*b/h*) as 10, 20, 50 with thickness h=1 is considered in the following examples. Four kinds of CNT distributions are taken into consideration one uniformly distributed (UD) and other three functionally graded (FG-V, FG-X, FG-O). For the sake of comparison the weight percent of CNT is considered to be same for all the four types of distributions. In the given numeric examples different non-dimensional quantities used are given in equation (46a-46d).

$$\bar{w} = \frac{w}{h}$$

$$\bar{\sigma}_{xx} = \frac{h^2}{q_0 a^2}\sigma_{xx}\left(\frac{a}{2},\frac{b}{2},\frac{h}{2}\right)$$

$$\bar{\tau}_{xy} = \frac{h^2}{q_0 a^2}\tau_{xy}\left(a, b, \frac{-h}{2}\right)$$

$$\bar{\tau}_{yz} = \frac{h}{q_0 a}\tau_{yz}\left(\frac{a}{2}, 0,0\right)$$

(4.2a-4.2d)

The non-dimensional centre deflection ($\bar{w}$) values for a square plates under uniformly distributed load for different CNT distributions, for different span to thickness ratios (*b/h*= 10, 20, 50) and an increasing volume fraction of CNTs is given in Table 4.5. The results are validated by comparing them with the results given by FSDT (Zhu *et al.*, 2012) and by 3-D elasticity theory (Alibeigloo and Liew, 2013). From the table it is clear that results are in close agreement. For the case of UDL the convergence occurs at *m*=*n*=13. It can be observed that the amount of deflection decreases with increase in the volume fraction of CNT. It can also be seen that the value for deflection is minimum in the case of FG-X followed by UD, FG-V and then FG-O. Hence it can be concluded that the CNT distribution pattern effects the overall stiffness of the plate. The distributions which are end heavy i.e. distributions having higher

CNT concentration at the ends (UD, FG-X) are more effective in enhancing the stiffness of the nanocomposite.

Table 4.5 Variation of non-dimensional central deflection *w/h* with CNT volume fraction (V_c^*) and width to thickness ratio (*b/h*) under a uniformly distributed load of q_0=1×10^5 N/m^2.

V_c^*	*b/h*		Present	FSDT Zhu *et al.* (2012)	ANSYS Zhu *et al.* (2012)	3-D solutions Alibeigloo and Leiw (2013)
0.11	10	UD	3.649×10^{-3}	3.739×10^{-3}	3.739×10^{-3}	3.617×10^{-3}
		FG-V	4.384×10^{-3}	4.466×10^{-3}	4.461×10^{-3}	4.455×10^{-3}
		FG-O	5.443×10^{-3}	5.230×10^{-3}	5.216×10^{-3}	-
		FG-X	3.046×10^{-3}	3.177×10^{-3}	3.176×10^{-3}	-
	20	UD	3.608×10^{-2}	3.628×10^{-2}	3.629×10^{-2}	3.621×10^{-2}
		FG-V	4.862×10^{-2}	4.879×10^{-2}	4.876×10^{-2}	4.872×10^{-2}
		FG-O	6.253×10^{-2}	6.155×10^{-2}	6.136×10^{-2}	-
		FG-X	2.665×10^{-2}	2.701×10^{-2}	2.703×10^{-2}	-
	50	UD	1.1554	1.155	1.155	1.15496
		FG-V	1.6536	1.653	1.652	1.6524
		FG-O	2.1637	2.157	2.150	-
		FG-X	0.7899	0.790	0.7915	-
0.14	10	UD	3.201×10^{-3}	3.306×10^{-3}	3.305×10^{-3}	3.295×10^{-3}
		FG-V	3.801×10^{-3}	3.894×10^{-3}	3.889×10^{-3}	3.883×10^{-3}
		FG-O	4.689×10^{-3}	4.525×10^{-3}	4.512×10^{-3}	-
		FG-X	2.736×10^{-3}	2.844×10^{-3}	2.842×10^{-3}	-
	20	UD	2.971×10^{-2}	3.001×10^{-2}	3.002×10^{-2}	2.990×10^{-2}
		FG-V	3.995×10^{-2}	4.025×10^{-2}	4.021×10^{-2}	4.013×10^{-2}
		FG-O	5.137×10^{-2}	5.070×10^{-2}	5.053×10^{-2}	-
		FG-X	2.229×10^{-2}	2.256×10^{-2}	2.258×10^{-2}	-
	50	UD	0.914	0.9175	0.9182	0.9174
		FG-V	1.321	1.326	1.325	1.325
		FG-O	1.7375	1.738	1.732	-
		FG-X	0.6252	0.6271	0.6284	-
0.17	10	UD	2.338×10^{-3}	2.394×10^{-3}	2.394×10^{-3}	2.383×10^{-3}
		FG-V	2.822×10^{-3}	2.864×10^{-3}	2.861×10^{-3}	2.854×10^{-3}
		FG-O	3.466×10^{-3}	3.378×10^{-3}	3.368×10^{-3}	-
		FG-X	1.981×10^{-3}	2.012×10^{-3}	2.011×10^{-3}	-
	20	UD	2.336×10^{-2}	2.348×10^{-2}	2.349×10^{-2}	2.34×10^{-2}
		FG-V	3.166×10^{-2}	3.174×10^{-2}	3.171×10^{-2}	3.166×10^{-2}
		FG-O	4.061×10^{-2}	4.020×10^{-2}	4.007×10^{-2}	-
		FG-X	1.714×10^{-2}	1.737×10^{-2}	1.738×10^{-2}	-
	50	UD	0.7526	0.7515	0.7521	0.7514
		FG-V	1.0829	1.082	1.081	1.078
		FG-O	1.4182	1.416	1.411	-
		FG-X	0.5150	0.5132	0.5141	-

Further a FGCNTRC plate is subjected to hydrostatic loading and the transverse shear deformation is evaluated for the simply supported boundary conditions. Table 4.6 describes the effect of addition of CNT in an isotropic plate. The properties of a CNTRC in the given formulation will represent those of an isotropic plate if we set the values of efficiency factors as one and volume fraction of CNT to be zero. It can be seen that 11% CNT reinforcement reduces the value of deflection by over 90%, further additions reduce the values even more. From the above two tables it is clear that FG-X and UD distributions are more effective in reducing the deflection of the plate, so it be concluded that deflection is least when the distribution of CNTs is more on the ends of the plate.

Table 4.6 Effect of CNT addition for a square plate with *b/h*=100 under hydrostatic loading load of $q_0 = 1\times10^5\ N/m^2$

V_c^*	UD	FG-V	FG-O	FG-X
0	102.7048	102.7048	102.7048	102.7048
0.11	8.9496	12.9442	16.9868	6.0297
0.14	7.0342	10.2936	13.5888	4.7192
0.17	5.8361	8.4851	11.1510	3.9309

Table 4.7 lists the values of normal and shear stresses in the case of uniformly distributed loading (UDL) for the above mentioned CNT distribution patterns, for different CNT volume fractions (V_c^*= 0.11, 0.14 0.17) and various values of span to thickness ratio. It is to be noted that while the CNT volume fraction does not have much impact on the stress value the stress values are clearly affected by the CNT distribution pattern. The values of stresses are more at the places with higher concentration of carbon nanotubes. The value $\bar{\sigma}_{xx}$ is higher for FG-X and UD distributions as the value of axial stress is being calculated at the top layer i.e. at $z=h/2$, while the values of $\bar{\tau}_{xy}$ $\bar{\tau}_{yz}$ are maximum for FG-O.

Table 4.7 Non-dimensional central deflection and stresses for a simply supported rectangular plate under uniformly distributed load of $q_0 = 1\times10^5\ N/m^2$

V_c^*	b/h	CNT Distribution	$\bar{\sigma}_{xx}\left(\frac{a}{2},\frac{b}{2},\frac{h}{2}\right)$	$\bar{\tau}_{xy}\left(a,b,\frac{-h}{2}\right)$	$\bar{\tau}_{yz}\left(\frac{a}{2},0,0\right)$
0.11	10	UD	0.96	1.369×10^{-2}	0.3622
		FG-V	1.834	1.72×10^{-2}	0.3884
		FG-O	0.058	2.126×10^{-2}	0.4456
		FG-X	1.329	1.191×10^{-2}	0.3219
	20	UD	0.85	0.956×10^{-2}	0.3293
		FG-V	1.634	1.329×10^{-2}	0.3635
		FG-O	0.049	1.661×10^{-2}	0.4200
		FG-X	1.141	0.756×10^{-2}	0.2834
	50	UD	0.815	0.844×10^{-2}	0.3188
		FG-V	1.573	1.219×10^{-2}	0.3562
		FG-O	0.0465	1.528×10^{-2}	0.4126
		FG-X	1.0801	0.641×10^{-2}	0.2699
0.14	10	UD	0.9999	1.198×10^{-2}	0.3502
		FG-V	1.9289	1.445×10^{-2}	0.3735
		FG-O	0.0480	1.766×10^{-2}	0.4364
		FG-X	1.3952	1.122×10^{-2}	0.3094
	20	UD	0.8597	0.794×10^{-2}	0.3126
		FG-V	1.6723	1.068×10^{-2}	0.3445
		FG-O	0.0393	1.322×10^{-2}	0.4062
		FG-X	1.1566	0.668×10^{-2}	0.2667
	50	UD	0.8153	0.685×10^{-2}	0.3000
		FG-V	1.5941	0.962×10^{-2}	0.3356
		FG-O	0.0367	1.197×10^{-2}	0.3972
		FG-X	1.0788	0.549×10^{-2}	0.2506
0.17	10	UD	0.9541	1.402×10^{-2}	0.3643
		FG-V	1.8299	1.689×10^{-2}	0.3908
		FG-O	0.0455	2.018×10^{-2}	0.4680
		FG-X	1.3280	1.367×10^{-2}	0.3161
	20	UD	0.8483	0.987×10^{-2}	0.3320
		FG-V	1.6392	1.318×10^{-2}	0.3668
		FG-O	0.0381	1.602×10^{-2}	0.4431
		FG-X	1.1440	0.865×10^{-2}	0.2785
	50	UD	0.8148	0.874×10^{-2}	0.3219
		FG-V	1.5813	1.212×10^{-2}	0.3599
		FG-O	0.0359	1.483×10^{-2}	0.4361
		FG-X	1.0838	0.731×10^{-2}	0.2653

Table 4.8 gives the values of displacement and stresses for separate values of volume fraction, for different CNT distributions and *b/h* ratios for a plate under hydrostatic loading. Results converge at $m=n=19$ for the case of hydrostatic loading, where, m and n are the index limits in equation 3.24. It can be seen that the values of deflection and axial stress are almost half of those obtained for uniformly distributed loads, but the values of shear stress are higher in the case of hydrostatic loading condition.

Table 4.8 Non-dimensional central deflection and stresses for a simply supported rectangular plate under hydrostatic loading with a maximum load of q_0=1×10^5 N

V_c^*	b/h	CNT distribution	$\bar{w}$	$\bar{\sigma}_{xx}\left(\frac{a}{2},\frac{b}{2},\frac{h}{2}\right)$	$\bar{\tau}_{xy}\left(a,b,\frac{-h}{2}\right)$	$\bar{\tau}_{yz}\left(\frac{a}{2},0,0\right)$
0.11	10	UD	1.824×10^{-3}	0.4792	2.051×10^{-2}	6.124×10^{-3}
		FG-V	2.192×10^{-3}	0.9154	2.376×10^{-2}	9.98×10^{-3}
		FG-O	2.721×10^{-3}	0.0287	2.622×10^{-2}	1.5×10^{-2}
		FG-X	1.523×10^{-3}	0.6634	1.91×10^{-2}	3.823×10^{-3}
	20	UD	1.804×10^{-2}	0.4242	1.735×10^{-2}	4.75×10^{-3}
		FG-V	2.431×10^{-2}	0.8159	2.148×10^{-2}	7.779×10^{-3}
		FG-O	3.127×10^{-2}	0.0244	2.339×10^{-2}	11.388×10^{-3}
		FG-X	1.333×10^{-2}	0.5697	1.532×10^{-2}	3.141×10^{-3}
	50	UD	0.5777	0.4071	1.645×10^{-2}	4.678×10^{-3}
		FG-V	0.8268	0.7862	2.087×10^{-2}	7.389×10^{-3}
		FG-O	1.0818	0.0232	2.259×10^{-2}	10.6×10^{-3}
		FG-X	0.395	0.5396	1.424×10^{-2}	3.27×10^{-3}
0.14	10	UD	1.6×10^{-3}	0.4994	1.884×10^{-2}	4.832×10^{-3}
		FG-V	1.9×10^{-3}	0.9634	2.108×10^{-2}	7.898×10^{-3}
		FG-O	2.345×10^{-3}	0.024	2.326×10^{-2}	11.85×10^{-3}
		FG-X	1.368×10^{-3}	0.6968	1.844×10^{-2}	3.117×10^{-3}
	20	UD	1.485×10^{-2}	0.4292	1.545×10^{-2}	3.862×10^{-3}
		FG-V	1.997×10^{-2}	0.8349	1.868×10^{-2}	6.095×10^{-3}
		FG-O	2.568×10^{-2}	0.0196	2.033×10^{-2}	8.792×10^{-3}
		FG-X	1.114×10^{-2}	0.5774	1.422×10^{-2}	2.64×10^{-3}
	50	UD	0.4573	0.4073	1.448×10^{-2}	3.91×10^{-3}
		FG-V	0.6606	0.7964	1.803×10^{-2}	5.858×10^{-3}
		FG-O	0.8687	0.0183	1.95×10^{-2}	8.223×10^{-3}
		FG-X	0.3126	0.5389	1.3×10^{-2}	2.821×10^{-3}
0.17	10	UD	1.17×10^{-3}	0.4762	2.083×10^{-2}	6.307×10^{-3}
		FG-V	1.411×10^{-3}	0.9134	2.291×10^{-2}	10.57×10^{-3}
		FG-O	1.733×10^{-3}	0.0226	2.511×10^{-2}	15.51×10^{-3}
		FG-X	0.9906×10^{-3}	0.6628	2.113×10^{-2}	4.137×10^{-3}
	20	UD	1.168×10^{-2}	0.4235	1.77×10^{-2}	4.869×10^{-3}
		FG-V	1.583×10^{-2}	0.8184	2.08×10^{-2}	8.257×10^{-3}
		FG-O	2.031×10^{-2}	0.019	2.26×10^{-2}	12.03×10^{-3}
		FG-X	0.869×10^{-2}	0.5711	1.697×10^{-2}	3.154×10^{-3}
	50	UD	0.3763	0.4071	1.682×10^{-2}	4.77×10^{-3}
		FG-V	0.5414	0.7901	2.023×10^{-2}	7.823×10^{-3}
		FG-O	0.7091	0.0179	2.187×10^{-2}	11.262×10^{-3}
		FG-X	0.2575	0.5415	1.577×10^{-2}	3.246×10^{-3}

Table 4.9 contains results for deflection and stresses for a square plate under sinusoidal loading conditions for the four CNT distribution patterns and different CNT volume fraction and plates span to thickness ratios. Here also it can be concluded that CNT introduction leads to significant decreases in the deflection values of the plate. The values of deflections are quite small in the case of sinusoidal loading as compares to UDL and HL conditions.

Table 4.9 Non-dimensional central deflection and stresses for a simply supported rectangular plate under a sinusoidal load of q_0=1×10^5 N

V_c^*	b/h	CNT distribution	$\bar{w}$	$\bar{\sigma}_{xx}\left(\frac{a}{2},\frac{b}{2},\frac{h}{2}\right)$	$\bar{\tau}_{xy}\left(a,b,\frac{-h}{2}\right)$	$\bar{\tau}_{yz}\left(\frac{a}{2},0,0\right)$
0.11	10	UD	2.461×10^{-3}	0.6571	1.54×10^{-2}	3.921×10^{-2}
		FG-V	2.919×10^{-3}	1.278	1.848×10^{-2}	4.883×10^{-2}
		FG-O	3.596×10^{-3}	0.0438	2.178×10^{-2}	6.305×10^{-2}
		FG-X	2.075×10^{-3}	0.9437	1.396×10^{-2}	3.124×10^{-2}
	20	UD	2.461×10^{-2}	0.5978	1.133×10^{-2}	2.843×10^{-2}
		FG-V	3.25×10^{-2}	1.129	1.498×10^{-2}	3.88×10^{-2}
		FG-O	4.138×10^{-2}	0.0374	1.762×10^{-2}	5.084×10^{-2}
		FG-X	1.851×10^{-2}	0.8155	0.973×10^{-2}	2.058×10^{-2}
	50	UD	0.7910	0.5751	1.008×10^{-2}	2.513×10^{-2}
		FG-V	1.106	1.0860	1.393×10^{-2}	3.57×10^{-2}
		FG-O	1.4318	0.0355	1.638×10^{-2}	4.714×10^{-2}
		FG-X	0.553	0.7776	0.797×10^{-2}	1.729×10^{-2}
0.14	10	UD	2.175×10^{-3}	0.7092	1.387×10^{-2}	3.53×10^{-2}
		FG-V	2.546×10^{-3}	1.3552	1.598×10^{-2}	4.357×10^{-2}
		FG-O	3.117×10^{-3}	0.0374	1.872×10^{-2}	5.663×10^{-2}
		FG-X	1.87×10^{-3}	0.998	1.336×10^{-2}	2.873×10^{-2}
	20	UD	2.048×10^{-2}	0.6116	0.968×10^{-2}	2.43×10^{-2}
		FG-V	2.695×10^{-2}	1.167	1.247×10^{-2}	3.32×10^{-2}
		FG-O	3.4308×10^{-2}	0.031	1.459×10^{-2}	4.395×10^{-2}
		FG-X	1.562×10^{-2}	0.8349	0.845×10^{-2}	1.78×10^{-2}
	50	UD	0.6345	0.5828	0.840×10^{-2}	2.09×10^{-2}
		FG-V	0.8932	1.112	1.14×10^{-2}	3.00×10^{-2}
		FG-O	1.1618	0.0291	1.337×10^{-2}	4.01×10^{-2}
		FG-X	0.4431	0.7864	0.694×10^{-2}	1.435×10^{-2}
0.17	10	UD	1.576×10^{-3}	0.6700	1.574×10^{-2}	3.982×10^{-2}
		FG-V	1.876×10^{-3}	1.273	1.798×10^{-2}	5.011×10^{-2}
		FG-O	2.29×10^{-3}	0.0357	2.071×10^{-2}	6.554×10^{-2}
		FG-X	1.3446×10^{-3}	0.9396	1.577×10^{-2}	3.214×10^{-2}
	20	UD	1.591×10^{-2}	0.5957	1.164×10^{-2}	2.908×10^{-2}
		FG-V	2.112×10^{-2}	1.1306	1.469×10^{-2}	4.015×10^{-2}
		FG-O	2.686×10^{-2}	0.0302	1.698×10^{-2}	5.357×10^{-2}
		FG-X	1.2×10^{-2}	0.8133	1.061×10^{-2}	2.116×10^{-2}
	50	UD	0.5142	0.5739	1.04×10^{-2}	2.58×10^{-2}
		FG-V	0.7225	1.0889	1.37×10^{-2}	3.71×10^{-2}
		FG-O	0.9381	0.0286	1.588×10^{-2}	4.997×10^{-2}
		FG-X	0.3585	0.7760	0.903×10^{-2}	1.774×10^{-2}

Table 4.10 gives the variation of deflection and stresses with different span to thickness ratios and CNT volume fractions for different CNT distributions under central point loading. The convergence for central point load occurs late than for hydrostatic loading and uniformly distributed loading at around m=n=29 (from equation 3.24). In case of central point loads the values of deflections and stress are least as compared to other stress distributions. One other

feature observed from the above mentioned tables is that the type of loading has no impact on the effectiveness of CNT inclusion. In all the different loading conditions a 6% increase in CNT concentration leads to around 36% reduction in deflection. Also the span to thickness ratio also has very less effect on CNT effectiveness. In all the three cases of *b/h* ratios (*b/h*=10, 20, 50) the percent reduction of deflection are 35-36% for a CNT increment of 6%.

Table 4.10 Non-dimensional central deflection and stresses for a simply supported rectangular plate under central point load with q_0=1×10^5 N

V_c^*	*b/h*	CNT distribution	$\bar{w}$	$\bar{\sigma}_{xx}\left(\frac{a}{2},\frac{b}{2},\frac{h}{2}\right)$	$\bar{\tau}_{xy}\left(a,b,\frac{-h}{2}\right)$	$\bar{\tau}_{yz}\left(\frac{a}{2},0{,}0\right)$
0.11	10	UD	1.65×10^{-4}	0.193	3.177×10^{-4}	1.481×10^{-4}
		FG-V	1.84×10^{-4}	0.369	4.23×10^{-4}	3.654×10^{-4}
		FG-O	2.221×10^{-4}	0.017	5.511×10^{-4}	9.528×10^{-4}
		FG-X	1.458×10^{-4}	0.282	2.615×10^{-4}	6.268×10^{-5}
	20	UD	4.005×10^{-4}	3.334×10^{-2}	4.027×10^{-5}	3.291×10^{-4}
		FG-V	4.862×10^{-4}	6.286×10^{-2}	6.881×10^{-5}	3.583×10^{-4}
		FG-O	5.968×10^{-4}	0.283×10^{-2}	9.639×10^{-5}	5.276×10^{-4}
		FG-X	3.259×10^{-4}	4.883×10^{-2}	2.382×10^{-5}	2.833×10^{-4}
	50	UD	1.936×10^{-3}	3.548×10^{-3}	4.585×10^{-6}	8.00×10^{-5}
		FG-V	2.495×10^{-3}	6.487×10^{-3}	9.134×10^{-6}	8.305×10^{-5}
		FG-O	3.11×10^{-3}	0.304×10^{-3}	1.334×10^{-5}	1.042×10^{-4}
		FG-X	1.464×10^{-3}	5.14×10^{-3}	1.939×10^{-6}	7.62×10^{-5}
0.14	10	UD	1.484×10^{-4}	0.208	2.667×10^{-4}	2.898×10^{-5}
		FG-V	1.64×10^{-4}	0.4005	3.44×10^{-4}	1.95×10^{-4}
		FG-O	1.97×10^{-4}	0.0155	4.46×10^{-4}	7.465×10^{-4}
		FG-X	1.33×10^{-4}	0.3054	2.402×10^{-4}	1.562×10^{-4}
	20	UD	3.475×10^{-4}	3.611×10^{-2}	2.82×10^{-5}	3.107×10^{-4}
		FG-V	4.185×10^{-4}	6.854×10^{-2}	4.972×10^{-5}	3.207×10^{-4}
		FG-O	5.137×10^{-4}	0.26×10^{-2}	7.093×10^{-5}	4.904×10^{-4}
		FG-X	2.856×10^{-4}	5.299×10^{-2}	1.722×10^{-5}	2.646×10^{-4}
	50	UD	1.625×10^{-3}	3.819×10^{-3}	2.744×10^{-6}	8.001×10^{-5}
		FG-V	2.09×10^{-3}	7.037×10^{-3}	6.131×10^{-6}	7.905×10^{-5}
		FG-O	2.62×10^{-3}	0.277×10^{-3}	9.358×10^{-6}	9.993×10^{-5}
		FG-X	1.227×10^{-3}	5.541×10^{-3}	9.073×10^{-6}	7.644×10^{-5}
0.17	10	UD	1.052×10^{-4}	0.1906	3.272×10^{-4}	1.662×10^{-4}
		FG-V	1.176×10^{-4}	0.3661	4.199×10^{-4}	4.085×10^{-4}
		FG-O	1.409×10^{-4}	0.0145	5.204×10^{-4}	1.069×10^{-3}
		FG-X	9.35×10^{-5}	0.2804	3.118×10^{-4}	7.522×10^{-5}
	20	UD	2.572×10^{-4}	2.289×10^{-2}	4.254×10^{-5}	3.318×10^{-4}
		FG-V	3.131×10^{-4}	6.221×10^{-2}	6.998×10^{-5}	3.667×10^{-4}
		FG-O	3.855×10^{-4}	2.445×10^{-2}	9.278×10^{-5}	5.696×10^{-4}
		FG-X	2.084×10^{-4}	4.833×10^{-2}	3.041×10^{-5}	2.63×10^{-4}
	50	UD	1.25×10^{-3}	3.504×10^{-3}	4.935×10^{-6}	7.997×10^{-5}
		FG-V	1.616×10^{-3}	6.43×10^{-3}	9.419×10^{-6}	8.4×10^{-5}
		FG-O	2.033×10^{-3}	0.27×10^{-3}	1.299×10^{-6}	1.097×10^{-4}
		FG-X	9.33×10^{-4}	5.064×10^{-3}	2.658×10^{-6}	7.248×10^{-5}

Figure 4.8 Shows variation of non-dimensional axial stress $\sigma_{xx}(a/2, b/2, z)$ with *z/h* for different distributions of CNT in the given plates with a volume fraction of 0.17. It can be noted from the Figure that the stress is almost zero at the top and the bottom for FG-O plates and at the bottom for FG-V plates because in these cases the value of CNT volume fraction is almost zero. It can also be noted that the curves are anti- symmetric for FG-O and FG-X distributions. It can be expected as the distributions themselves are anti symmetric. It can also be pointed out that compressive stress is maximum for FG-O distribution while the tensile stress is maximum for FG-X distribution.

Plot of non-dimensional shear stress ($\bar{\tau}_{yz}$) against non-dimensional thickness of the plate is given in Figure 4.9. The analyses is made on a FGCNTRC plate with span to thickness ratio *a/h*=50 and the volume fraction of CNT is equal to 0.11. Different CNT distribution schemes are taken into account and results are plotted for the case of a sinusoidal loading condition. It is observed that the values of shear stress are zero at the top and the bottom surface and the maximum arrives at the neutral axis which is the expected distribution, hence validating the use of IHSDT for this analyses. For the CNT distributions symmetric about the centre of the plate (UD, FG-X, FG-O) the neutral axis falls at middle of the plate but for the case of FG-V it lies of the mid plane.

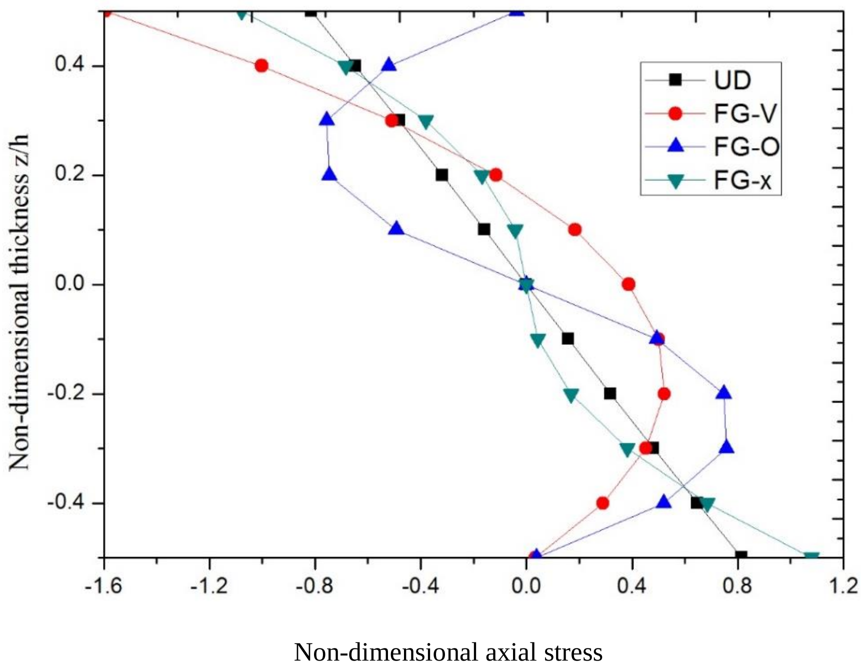

Figure 4.8 Variation of non-dimensional axial stress $\sigma_{xx}(a/2, b/2, z)$ with non-dimensional depth (*z/h*)

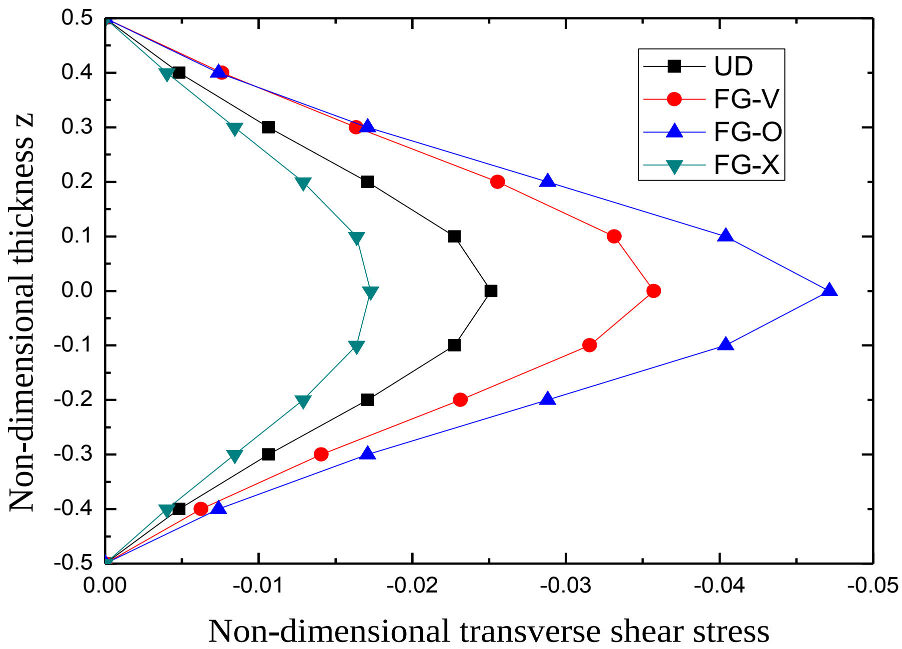

Figure 4.9. Variation of non-dimensional transverse shear stress $\bar{\tau}_{yz}(a/2,0,h)$ with non-dimensional thickness for thickness ratio *a/h*=50 and a CNT volume fraction of $V_c^* = 0.11$ under sinusoidal loading.

Figures 4.10a-4.10d shows the variation of non-dimensional axial deflection with w/h for UDL and SSL loading conditions for volume fraction of CNT being 0.11. Graphs are plotted for the variation of non-dimensional deflection with span to thickness ratio different CNT distribution schemes and observations are made accordingly. It can be noted that deflection is more in the case of UDL loading as compared to SSL. It can also be noted that the deflection is maximum in the case of FG-O distribution and minimum in the case of FGV distribution.

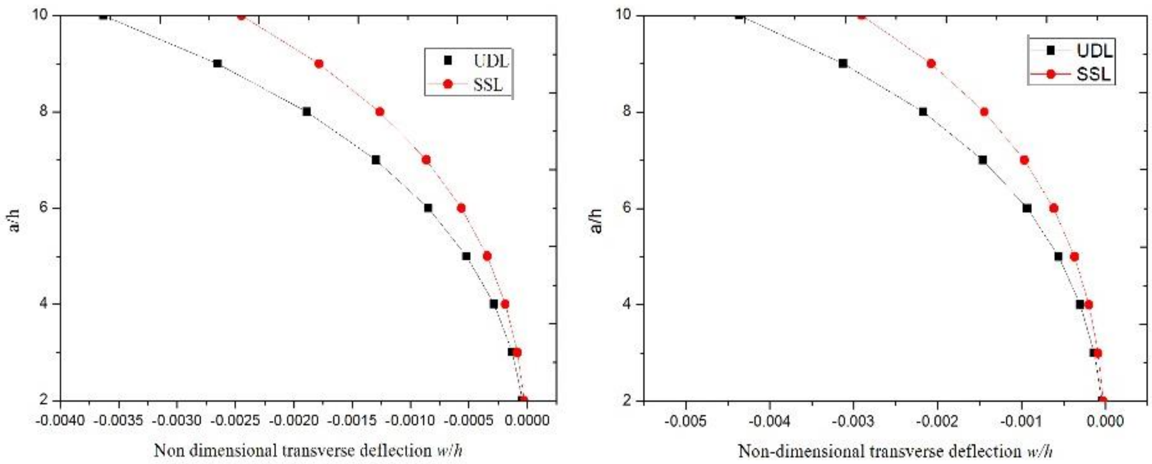

a

b

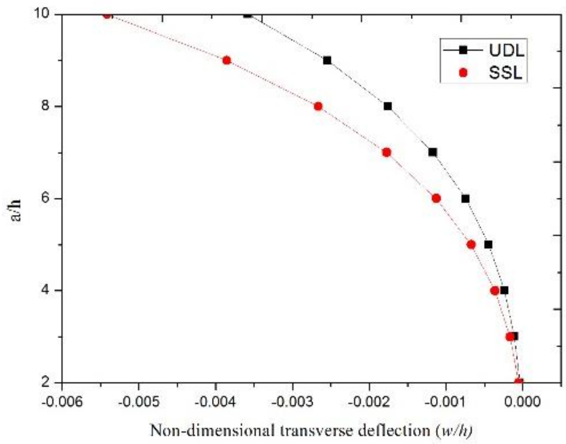

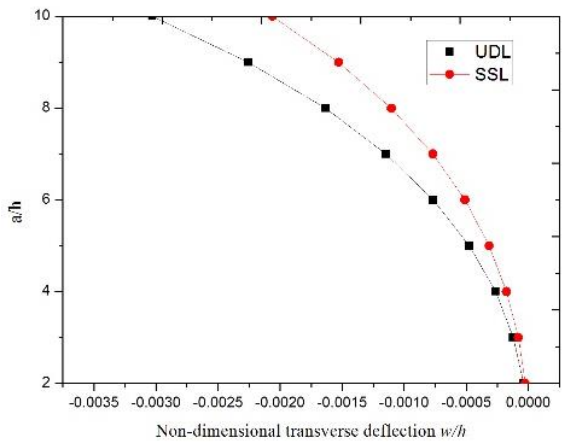

c d

Figure 4.10 Variation of non-dimensional axial deflection with span to thickness ratio for a FGCNTC platefor uniformly distributed and sinusoidally varying loads, (a) UD (b) FGVCNT (c) FGOCNT (d) FGXCNT.

4.5. Analysis of FGCNTRC Plates using Isogeometric Analysis

Results for isogeometric analysis of a functionally graded carbon nanotube reinforced nanocomposite are presented in this section for different boundary conditions and different CNT orientations.

Figure 4.11 shows the effect of CNT distribution pattern on the convergence rate for isogeometric analysis of a FGCNTRC with span to thickness ratio a/h=10. A plate with equal dimensions in x and y coordinate directions is taken into account and the volume fraction of CNT in the plate is taken equal to 0.11. It can be seen that results for FG-O of CNT converge slower than the other configurations. This shows the effect of inhomogeneity in CNT reinforced composite plates.

Figure 4.12 illustrates the effect of CNT volume fraction on the rate of convergence of results for the case of static analysis of FGM plate. Square plate with FGV type of FGM distribution along the thickness coordinate is taken into account and graphs are plotted for an increasing volume fraction of carbon nanotubes. Figure makes it clear that convergence comes at a much faster rate for CNT reinforced composite plates in comparison to those with no reinforcement. This is understandable from the fact that the value of Young's modulus and other constants in the constitutive equations become very high when a structure is reinforced with carbon nanotubes.

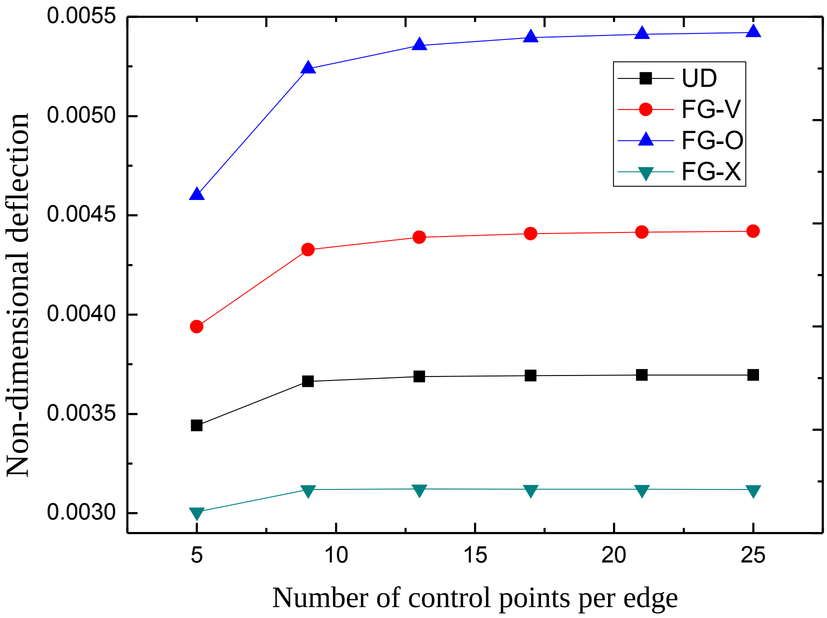

Figure 4.11 Effect of CNT distribution scheme on the convergence rate for a FGCNTRC plates with *b/h*=10 and $V_c^* = 0.11$.

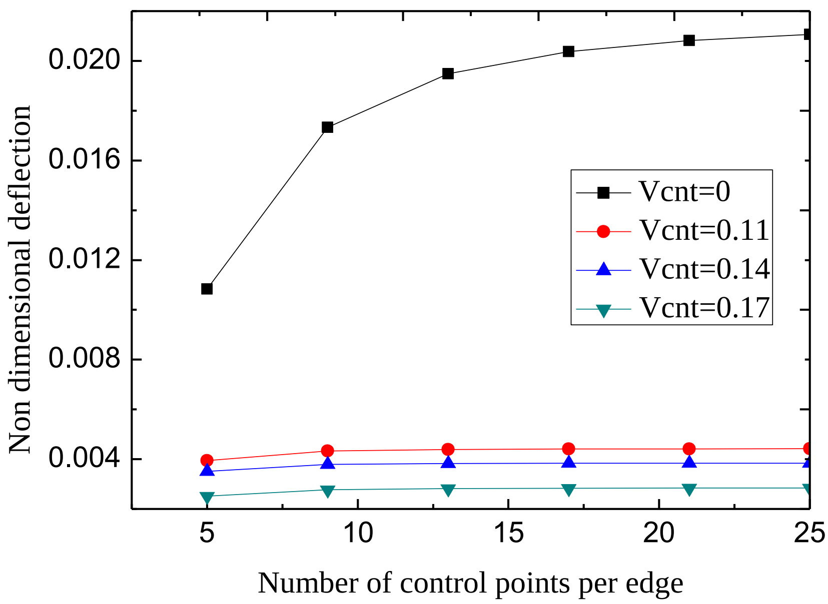

Figure 4.12 Effect of CNT distribution scheme on the convergence rate for a FGVCNTRC plates with *b/h*=10

Results for the non-dimensional transverse deflection for different boundary conditions for a FGCNTRC plate are listed in Table 4.11. Volume fraction of CNT is taken to be 0.11 and a uniformly distributed load with q_0=1×10^5 N. Cases with all edges simply supported, all edges clamped and two edges clamped and two edges simply supported is considered in this analysis. Results for the case of all edges simply supported are validated by comparing them with those of exact analysis and results for two analyses are very close, hence validating the given formulation. Another observation from the table is that the values decreases with an increase in the number clamped edges, this can be explained by the fact that a higher number of degrees of freedoms are arrested when an edge is made clamped.

Table 4.12 provides an analyses of deflection results for a functionally graded CNT reinforced plate having a CNT volume fraction of 0.14. The plate is under a uniformly distributed load of q_0=1×10^5 N. FGV distribution scheme is adopted to arrive at these values. Results are presented for values of deflection under separate boundary conditions.

Table 4.11 Non-dimensional central deflection for a square FGCNTRC plate with V_c^*=0.11 under different boundary conditions.

b/h		SSSS (IGA)	SSSS (Analytical)	CCCC (IGA)	CSCS (IGA)
10	UD	3.695×10^{-3}	3.649×10^{-3}	2.09×10^{-3}	3.265×10^{-3}
	FG-V	4.41×10^{-3}	4.384×10^{-3}	2.221×10^{-3}	3.782×10^{-3}
	FG-O	5.421×10^{-3}	5.443×10^{-3}	2.57×10^{-3}	4.505×10^{-3}
	FG-X	3.119×10^{-3}	3.046×10^{-3}	1.96×10^{-3}	2.804×10^{-3}
20	UD	3.621×10^{-2}	3.608×10^{-2}	1.306×10^{-2}	3.307×10^{-2}
	FG-V	4.84×10^{-2}	4.862×10^{-2}	1.553×10^{-2}	4.217×10^{-2}
	FG-O	6.172×10^{-2}	6.253×10^{-2}	1.909×10^{-2}	5.196×10^{-2}
	FG-X	2.69×10^{-2}	2.665×10^{-2}	1.113×10^{-2}	2.538×10^{-2}

Results for the simply supported boundary condition are validating by matching them against those obtained via analytical framework using Navier solutions. Numeric results are found to be very close to results obtained using analytical framework.

Table 4.12 Non-dimensional deflection for a FGCNT reinforced plate with V_c^*=0.14 and under a uniformly distributed load of $q_0=1\times10^5$ *N*.

b/h		SSSS (IGA)	SSSS (Analytical)	CCCC (IGA)	CSCS (IGA)
10	UD	3.253×10^{-3}	3.201×10^{-3}	1.942×10^{-3}	2.911×10^{-3}
	FG-V	3.842×10^{-3}	3.801×10^{-3}	2.043×10^{-3}	3.343×10^{-3}
	FG-O	4.676×10^{-3}	4.689×10^{-3}	2.335×10^{-3}	3.975×10^{-3}
	FG-X	2.805×10^{-3}	2.736×10^{-3}	1.84×10^{-3}	2.538×10^{-3}
20	UD	2.992×10^{-2}	2.971×10^{-2}	1.155×10^{-2}	2.784×10^{-2}
	FG-V	3.993×10^{-2}	3.995×10^{-2}	1.352×10^{-2}	3.563×10^{-2}
	FG-O	5.093×10^{-2}	5.137×10^{-2}	1.643×10^{-2}	4.418×10^{-2}
	FG-X	2.260×10^{-2}	2.229×10^{-2}	1.006×10^{-2}	2.153×10^{-2}

In Table 4.13 non-dimensional central displacement values are calculated for a CNT reinforced composite plate acted upon by a uniformly distributed load of $q_0=1\times10^5$ *N*, in the transverse direction. The plate has a FGV CNT distribution scheme and volume fraction of CNT reinforcements is 0.17. Analysis is carried out using a NURBS basis function of degree 1 and results are validated for simply supported condition by comparing the values with those of analytical results.

Table 4.13 Non-dimensional deflection for a FGCNT reinforced plate with V_c^*=0.17 and under a uniformly distributed load of $q_0=1\times10^5$ N

b/h		SSSS (IGA)	SSSS (Analytical)	CCCC (IGA)	CSCS (IGA)
10	UD	2.367×10^{-3}	2.338×10^{-3}	1.334×10^{-3}	2.08×10^{-3}
	FG-V	2.841×10^{-3}	2.822×10^{-3}	1.417×10^{-3}	2.420×10^{-3}
	FG-O	3.452×10^{-3}	3.466×10^{-3}	1.619×10^{-3}	2.876×10^{-3}
	FG-X	2.015×10^{-3}	1.981×10^{-3}	1.25×10^{-3}	1.79×10^{-3}
20	UD	2.343×10^{-2}	2.336×10^{-2}	0.836×10^{-2}	2.133×10^{-2}
	FG-V	3.148×10^{-2}	3.166×10^{-2}	1.007×10^{-2}	2.724×10^{-2}
	FG-O	4.006×10^{-2}	4.061×10^{-2}	1.212×10^{-2}	3.368×10^{-2}
	FG-X	1.752×10^{-2}	1.741×10^{-2}	0.719×10^{-2}	1.636×10^{-2}

4.6. Summary

Bending response of functionally graded plates having two isotropic phases and functionally graded carbon nanotube reinforced composite plates has been examined using IHSDT. The close form solutions are obtained for simply supported plates subjected to various transverse loading conditions. The various transverse loads considered in this study are uniform load, sinusoidal load, central point load and hydrostatic load. Moreover the effect of power law index, span to thickness ratio, CNT volume fraction and their distribution on the bending response are observed. It should be noted that the analytical solutions are limited for simply supported boundary conditions. Therefore, numerical solutions in isogeometric framework are developed and the results are compared with the analytical results. It is observed that the present numerical results agree well with the independently obtained analytical results.

Chapter 5

Conclusions and Scope for Future Work

In this section conclusions are drawn from studying the results for the bending behaviour of functionally graded composite plates of two kinds. Analyses done in analytical as well as IGA framework for both kinds of plate. Results are validated by comparing them with standard results present in the literature. Following Conclusions can be made from those observations.

1. The inverse hyperbolic shear deformation theory gives very accurate results, when applied to study behaviour of different kinds of functionally graded plates. The results are comparable with those obtained by using quasi 3-D theory.
2. The CNT reinforcements improves the response of plates towards bending under transverse loading. The deflection reduces by upto 80% when compared with results of bending analysis of isotropic plates.
3. The effect of geometric parameters like the length to width ratio, span to thickness ratio etc. is clearly visible on the values of deflection and stresses. Value of deflection decreases with an increases in the value of span to thickness ratio but becomes constant after reaching a certain value.
4. The geometric and reinforcement factors have a significant impact on the convergence rate in the case of isogeometric analyses. Convergence is attained at very less number of elements for the IG analyses of CNT reinforced composite materials.
5. The gradation parameters like the power law index and CNT distribution have a significant impact on the bending behaviour of structural members. Therefore, the gradation of properties have a great impact in improving the tailorability of the materials. An increase in the value of power law index leads to increase in the value of deflection and alters the trends in stress values significantly.

Publications from the present work

Soni A, Grover N, Bhardwaj G. Analytical solution for the bending behaviour of carbon nanotube reinforced composite plate, under preparation.

Soni A, Grover N, Bhardwaj G. Isogeometric modelling of FG and FGCNTRC plates, under preparation.

Soni A, Grover N, Bhardwaj G. Analytical solution for bending analysis of functionally graded plates using secant function based shear deformation theory, 3rd Indian Conference on Applied Mechanics (INCAM), MNNIT Allahabad 2017;162:25-26.

Scope for future work

Study of FGM structures under hygro-thermal environment to analyse their static, and dynamic response.

Study of composite structure with multiple reinforcements and reinforcement of CNT in functionally graded matrices.

Developing a GUI based on the framework of IGA.

References

Aragh BS, Barati AHN, Hedayati H. Eshelby-Mori-Tanaka approach for vibrational behavior of continuously graded carbon nanotube-reinforced cylindrical panels. Compos Part B-Eng 2012;43:1943-54.

Alibeigloo A, Liew KM. Thermoelastic analysis of functionally graded carbon nanotube-reinforced composite plate using theory of elasticity. Compos Struct 2013;106:873-81.

Arani AG, Haghparast E, Maraghi ZK, Amir S. Static stress analysis of carbon nanotube reinforced composite (CNTRC) cylinder under non-axisymmetric thermo-mechanical loads and uniform electro-magnetic fields. Compos Part B-Eng 2015;68:136–145.

Aydogdu M. A new shear deformation theory for laminated composite plates. Compos Struct 2009;89:94–101.

Bhardwaj G, Upadhyay AK, Pandey R, Shukla KK. Non-linear flexural and dynamic response of CNT reinforced laminated composite plates. Composites: Part B 2013; 45:89–100

Birman V, Byrd LW. Modeling and analysis of functionally graded materials and structures. ASME Appl Mech Rev 2007;60:195–216.

Carrera E, Brischetto S, Robaldo A. Variable kinematic model for the analysis of functionally graded material plates. AIAA J 2008;46:194–203.

Chi SH, Chung YL. Mechanical behavior of functionally graded material plates under transverse load. Part I: analysis. Int J Solids Struct 2006;43:3657–74.

Chi SH, Chung YL. Mechanical behavior of functionally graded material plates under transverse load. Part II: numerical results. Int J Solids Struct 2006;43:3675–91.

Croce LD, Venini P. Finite elements for functionally graded Reissner–Mindlin plates. Comput Methods Appl Mech Eng 2004;193:705–25.

Feldman E, Aboudi J. Buckling analysis of functionally graded plates subjected to uniaxial loading. Compos. Struct. 1997;38:29–36.

Formica G, Lacarbonara W, Alessi R. Vibrations of carbon nanotube-reinforced composites. J Sound Vib. 2010;329:1875-89.

Gibson RF. Principles of composite material mechanics. New York: McGrawHill Publications; 1994.

Grover N, Maiti DK, Singh BN. A new inverse hyperbolic shear deformation theory for static and buckling analysis of laminated composite and sandwich plates. Compos Struct 2013;95: 667–75.

Grover N, Maiti DK, Singh BN. New non-polynomial shear–deformation theories for the structural behavior of laminated-composite and sandwich plates. AIAA J 2013;95:667–75.

Hughes TJR, Cottrell JA, and Bazilevs Y. Isogeometric Analysis: CAD, Finite Elements, NURBS, Exact Geometry and Mesh Refinement. Computer Methods in Applied Mechanics and Engineering. 2005;194:4135–4195.

Iijima S. Helical microtubes of graphitic carbon. Nature 1991;354:56-8.

Jafari MS, Sobhani AB, Khoshkhahesh V, Taherpour A. Mechanical buckling of nanocomposite rectangular plate reinforced by aligned and straight single-walled carbon nanotubes. Compos Part B-Eng 2012;43:2031-40.

Javaheri R, Eslami M. Buckling of functionally graded plates under in-plane compressive loading. J. Appl Math Mech 2002;82:277–283.

Jha DK, Kant T, Singh RK. A critical review of recent research on functionally graded plates. Compos Struct 2013;96:833–49.

Kant T, Ravichandran RV, Pandya BN, Mallikarjuna. Finite element transient dynamic analysis of isotropic and fibre reinforced composite plates using a higher-order theory. Compos Struct 1988;9:319–42.

Kashtalyan M. Three-dimensional elasticity solution for bending of functionally graded plates. Eur J Mech A/Solid 2004;23:853–64.

Kreupl F, Graham AP, Liebau M, Duesberg GS. Seidel R, Unger E, "Carbon nanotubes for interconnect application" Infineon technologies AG, Corporate research, Otto-Hahn-Ring 6, 81739 Munich, Germany.

Kulkarni K, Singh BN, Maiti DK. Analytical solution for bending and buckling analysis of functionally graded plates using inverse trigonometric shear deformation theory, Compos Struct 134;147–157.

Liew KM, Lei ZX, Zhang LW. Mechanical analysis of functionally graded carbon nanotube reinforced composites: A review. Compos Struct 2015;120:90-7.

Love AEH. The mathematical theory of elasticity, 4th edition. Cambridge University Press, Cambridge; 1927.

Mantari JL, Soares CG. Generalized hybrid quasi-3-D shear deformation theory for the static analysis of advanced composite plates. Compos Struct 2012;94:2561–75.

Mantari JL, Oktem AS, Soares CG. A new trigonometric shear deformation theory for isotropic, laminated composite and sandwich plates. Int J Solids Struct 2012;49:43–53.

Mindlin RD. Influence of rotary inertia and shear on flexural motions of isotropic elastic plates. J App Mech 1951;18:31 –8.

Murthy MVV. An improved transverse shear deformation theory for laminated anisotropic plates. NASA Technical Paper; 1981

Natarajan S, Haboussi M, Manickam G. Application of higher-order structural theory to bending and free vibration analysis of sandwich plates with CNT reinforced composite facesheets. Compos Struct 2014;113:197-207.

Pagano NJ. Exact solutions for rectangular bidirectional composites and sandwich plates. Compos Mater 1970;4(1):20–34.

Pan E. Exact solution for functionally graded anisotropic elastic composite laminates. Compos Mater 2003;37:1903–20.

Praveen, G.N., Reddy, J.N.: Nonlinear transient thermoelastic analysis of functionally graded ceramic-metal plates. Int. J. Solids Struct 35, 4457–4476 (1998)

Reddy JN. A simple higher order shear deformation theory for laminated composite plates. Appl Mech 1984;51:752–4.

Reddy JN. Mechanics of laminated composite plates and shells: theory and analysis. Boca Raton, FL: CRC Press, 2004.

Reissner E. The effect of transverse shear deformation on the bending of elastic plates. App Mech 1945;12(2):69–77.

Reissner E, Stavsky Y. Bending and stretching of certain type of heterogeneous elastic plates. Appl Mech 1951;9:402-08.

Shen SH. Nonlinear bending of functionally graded carbon nanotube-reinforced composite plates in thermal environments. Compos Struct 2009;91:9-19.

Srinivas S, Rao AK. Bending, vibration and buckling of simply supported thick orthotropic plates and laminates. Int J Solids Struct 1970;6:1463–81.

Srinivas S, Joga Rao CV, Rao AK. An exact analysis for vibration of simply supported homogeneous and laminated thick rectangular plates. J Sound Vib 1970;12:187–99.

Swaminathan K, Patil SS. Higher order refined computationalmodelwith12 degrees of freedom for the stress analysis of antisymmetric angle-ply plates— analytical solutions. Compos Struct 2007;80:595–608.

Talha, M, Singh, BN. Static response and free vibration analysis of FGM plates using higher order shear deformation theory. Appl Math Model 2010;34:3991–4011

Thai HT, Kim SE, A simple higher-order shear deformation theory for bending and free vibration analysis of functionally graded plates. Compos Struct 2013;96:165–173.

Tran LV, Ferreira AJM, Nguyen H. Isogeometric analysis of functionally graded plates using higher-order shear deformation theory. Composites: Part B 2013; http: //dx.doi.org /10.1016/j .compositesb.2013.02.045

Touratier M. An efficient standard plate theory. Int J Eng Sci 1991;29(8):745–52.

Valizadeh N, Natarajan S, Gonzalez-Estrada OA, Rabczuk T, Bui TQ, Bordas SP. NURBS-based finite element analysis of functionally graded plates: static bending, vibration, buckling and flutter, Composite Structures 2012;doi:http://dx.doi.org/10.1016/j.compstruct.2012.11.008.

Walpole LJ. On the overall elastic moduli of composite materials. J Mech Phys Solids. 1969; 17:235–51.

Wanga J, Pyrz R. Prediction of the overall moduli of layered silicate-reinforced nanocomposites—part I: basic theory and formulas. Compos Sc and tech 2004;925-934.

Wu CP, Li HY. An rmvt-based third-order shear deformation theory of multilayered functionally graded material plates. Compos. Struct 2010;92(10):2591–2605.

Wu CP, Chiu, KH. Rmvt-based meshless collocation and element-free Galerkin methods for the quasi-3-D free vibration analysis of multilayered composite and FGM plates. Compos. Struct 2011;93(5):1433–1448.

Zenkour, A.M.: Generalized shear deformation theory for bending analysis of functionally graded materials. Appl. Math. Model 30,67–84 (2006)

Zenkour AM. Benchmark trigonometric and 3-D elasticity solutions for an exponentially graded thick rectangular plate. Arch Appl Mech 2007;77:197–214.

Zhang LW, Lei ZX, Liew KM, Yu JL. Static and dynamic of carbon nanotube reinforced functionally graded cylindrical panels. Compos Struct 2014;111:205-12.

Zhang CL, Shen HS. Temperature-dependent elastic properties of single-walled carbon nanotubes: prediction from molecular dynamics simulation. Appl Phys Lett 2006:89.

Zhu P, Lei ZX, Liew KM. Static and free vibration analyses of carbon nanotube reinforced composite plates using finite element method with first order shear deformation plate theory. Compos Struct 2012;94:1450-60.

Web references

https://upload.wikimedia.org/wikipedia/commons/c/c5/KaiyuanBowStrung.jpg

http://www.compositesworld.com/news/dutch-bridge-claims-to-be-largest-single-span-composite-bridge-in-the-world

http://d2n4wb9orp1vta.cloudfront.net/cms/IMG_4992_500.jpg;width=560.